Chapter 2

Solutal Marangoni convection due to desorption of acetone from V-shaped containers in microgravity and normal gravity conditions: experimental results.

2.1 Introduction

The research described in this thesis is focused on the use of microgravity experiments as a tool for understanding the relationship between solutal Marangoni convection and mass transfer. As described in chapter 1, Marangoni convection can enhance the mass transfer coefficient as it is responsible for enhancing the rate of solute transport from the bulk of a liquid to the gas-liquid interface. The convective patterns originating from Marangoni convection in shallow layers (of the order of 10^{-3}-10^{-4} m), which are interesting from an engineering point of view, are hard to study, even with the help of advanced techniques, such as Laser-Doppler anemometry [1]. Convection patterns can be studied easier in deeper layers (of the order of 10^{-2} m), but in these layers Rayleigh convection also contributes to the convective pattern unless gravity is reduced.

In this chapter, the development of solutal Marangoni convection in microgravity is studied, and flow and concentration patterns are compared to those found in normal gravity. As a model system, the desorption of acetone from water into air has been chosen. This system is stationary unstable with respect to the Sternling-Scriven criteria [2]. Systems with various geometries (V-shaped containers) have been used in order to make comparisons between micro- and macroconvective patterns. This chapter is focused on understanding the development of the flow pattern and the concentration distribution in the liquid qualitatively. A quantitative comparison between the experiments and a numerical model is presented in chapter 3. This numerical model is used to predict the influence of the Marangoni convection on the mass transfer coefficient in chapter 4.

In section 2.2, the V-shaped containers are described in more detail, followed by an outline of the timeline of the microgravity experiments and the hardware used for the experiments. Interferometry was used to determine concentration patterns in the V-shaped containers. This technique and the way it was implemented in the experiments is described in detail in section 2.3. In section 2.4, the results of sounding rocket experiments are presented, and in section 2.5 the results of 1-g experiments. Some parabolic flight experiments are described in section 2.6. Finally, the results are discussed in section 2.7, and the conclusions presented in section 2.8.

2.2 Experimental

The system

The geometry that has been chosen to study the solutal Marangoni convection is a V-shaped container with either a flat, a convex or a concave interface. Initially, these V-shaped containers were selected to represent abstractions for dead zones in packed columns, but by choosing various interface shapes it is also possible to study micro- as well as macroconvective patterns as they might occur in shallow films. The V-shaped containers are constructed of quartz. The eight different containers that have been used are depicted in figure 1. The shaded areas are the open sides of the containers. When liquid is injected through the bottom of the container, a liquid-gas interface is created with the exact form of these shaded areas, provided the appropriate amount of liquid is introduced. The liquid used is a 5 wt % acetone in water solution. Acetone is allowed to evaporate from the containers into continuously refreshed air. Overflow of the container is prevented by coating the top of the quartz walls of the container with a Teflon layer. In figure 1, these layers are represented by the thick black lines. The length of the diagonal side walls is 2 cm for each container, except for container 4, whose diagonal side wall is 1.41 cm long. The vertical distance between the bottom of the container and the interface is 1.41, 2.00, 1.19, 1.50, 1.41, 1.59, 2.00 and 2.10 cm respectively. The internal width of the container is 0.5 cm in all cases, except for container 5, which has an internal width of 1 cm.

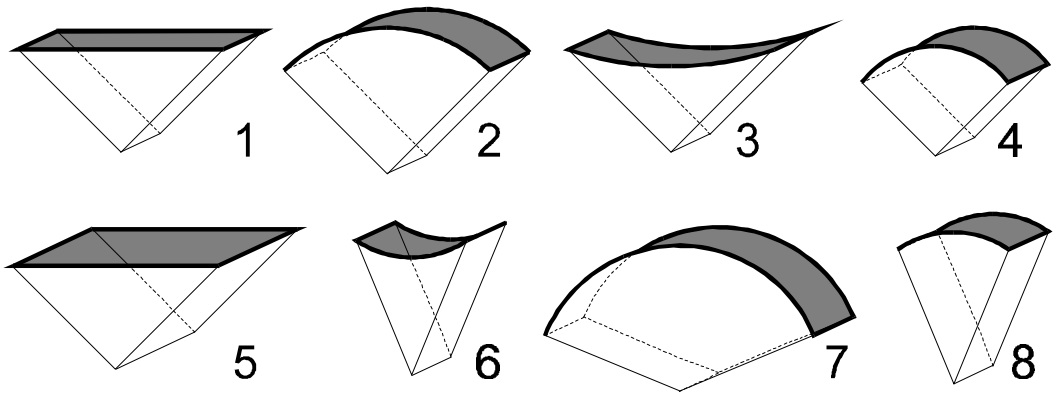

figure 1 *Sketch of the eight different containers used in the experiments. The shaded areas represent the free gas-liquid interfaces. Teflon layers are indicated by thick black lines.*

Timeline of microgravity experiments

Previous experiments involving V-shaped containers have been performed by Hoefsloot et al. [3] during parabolic flights. Preliminary results were obtained and a sounding rocket experiment was scheduled for April 1992. The experiment was launched as FSM-D on board of Maser 5 from the launch site Esrange in Kiruna, Sweden. Due to a hardware failure, this experiment needed to be reflown and was flown finally as FSM-5 on board of Texus-32 from

Esrange. This rocket was launched on May 5, 1994. In between the two sounding rocket experiments, parabolic flight experiments were performed on board of the Caravelle during the 16th ESA parabolic flight campaign in January 1993 [4]. This parabolic flight opportunity was used to prepare the Texus flight, but also served as a scientific opportunity. Some results of these parabolic flights are described in section 2.6.

Liquids were inserted in the FSM-5 module three days prior to launch. Texus-32 reached an altitude of 238844 meter and microgravity was achieved between 77 and 423 seconds after launch (a total of 5 minutes and 46 seconds). Microgravity levels were excellent and less than 10^{-4} g.

The 16th ESA parabolic flight campaign lasted three days with one flight each day. Each flight consisted of 31 parabolas. Liquids had to be refreshed and set-ups to be cleaned in between flights. Microgravity levels were around 10^{-2} g for each parabola and microgravity time was between 20 and 25 seconds. In the pull-up phases before and after each parabola gravity levels were around 1.8 g.

Hardware for sounding rocket experiment

A photo of the internals of the FSM-5 module can be seen in figure 2. The module consisted of three plates that were suspended from six metal rods. These rods were attached to the rocket skin through flexible, but tight, bearings. This construction prevented the plates, which contained the interferometry optics, to bend during flight. The large temperature difference between skin and internals might otherwise cause a slight deformation, sufficient to misalign the laser optics. Furthermore, this construction helped to minimise the conductive heat flux from the skin to the internals. The inside of the skin was coated with a cork-like material for further isolation, and radiation shields were inserted to reduce the radiative heat flux.

Two plates contained identical experimental set-ups and one plate contained all the necessary electronics. The experimental plates consisted of a cell house, laser optics, a liquid injection unit and an air circulation system. Four containers were positioned in each of the cell houses. Containers 1 to 4 were accommodated in cell house X and containers 5 to 8 were accommodated in cell house Y. A sketch of the positioning of the containers within a cell house can be seen in figure 3. Liquid could be injected via inlets in the cell houses into the containers using the liquid injection unit. A small injection needle was present in the container that was designed in such a way that liquid would be squeezed against the quartz wall of the container and would not escape from the container during injection in microgravity. The quartz containers (optical quality; Hellma) were coated on the top with a black Teflon layer to prevent liquid overflow. On the outside they were coated with an anti-reflection layer to avoid double interference patterns. On top of the containers deldrin pieces were placed that created an air space above the liquid of the same size as the depth of the container and of the same shape as the interface (see figure 3). The deldrin pieces were covered with a deldrin net with a fine maze width. Outside this confined air space, air was recirculated. The net intended to prevent forced

air flow in the confined air space above the container and any forced flow in the liquid as a result of this.

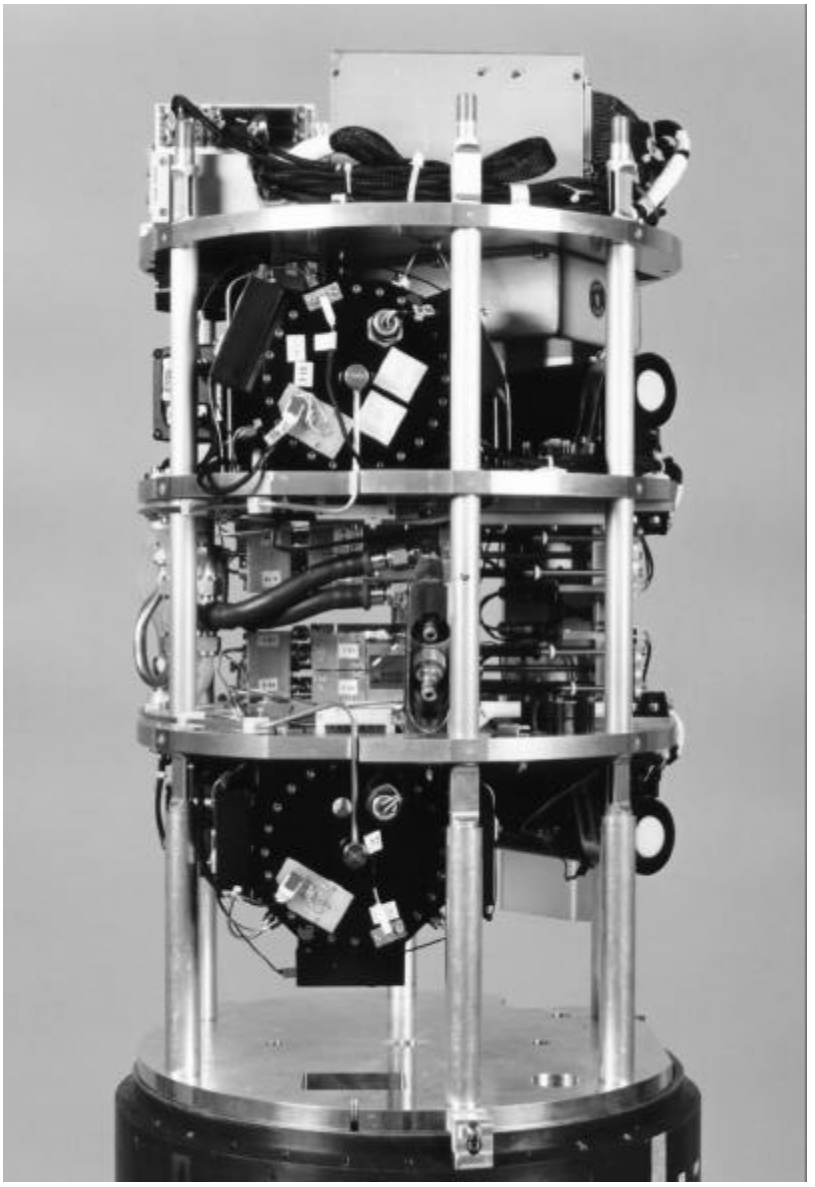

figure 2 Photo of the internals of the FSM-5 module.

The air circulation system consisted of an air pump, a filter housing containing an active carbon filter, a tube system and the internals of the cell house. The system was designed to recycle the air fast enough to maintain the acetone concentration in the cell house outside the confined air space at a value close to zero. This was achieved by pumping the air through the carbon filter, using a flow of 5 l/min (volume cell house approximately 0.6 l).

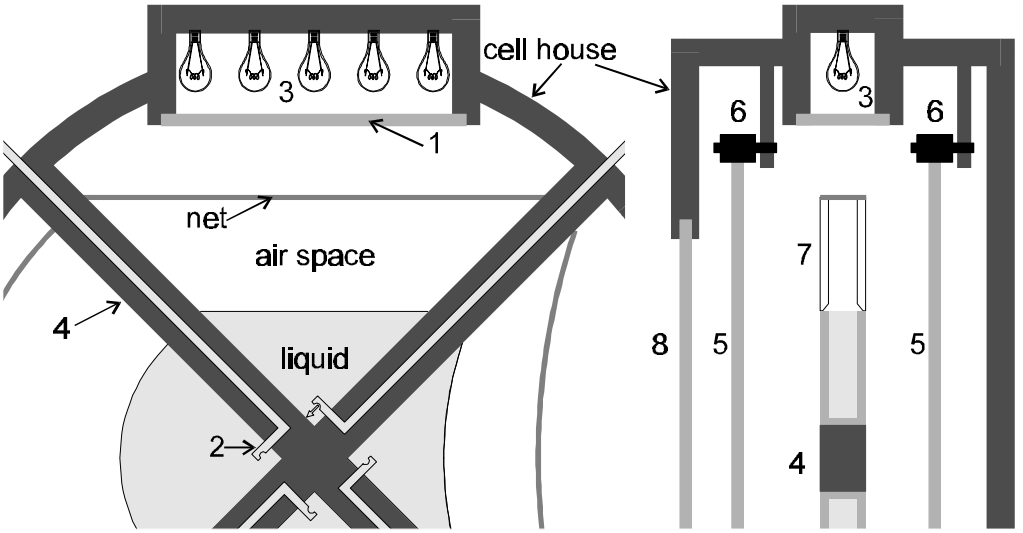

figure 3 *Sketch of the position of a container within the cell house. 1 = cold mirror; 2 = liquid injection tube; 3 = lamps; 4 = metal cross; 5 = semi-reflective mirror; 6 = adjusting screw; 7 = deldrin piece creating the air space; 8 = positive lens*

The optical system consisted of the cell house, a laser and a power supply, a semi-reflective mirror, and a camera. The system is sketched in figure 4. In section 2.3, the principle of interferometry is explained. Here, only the hardware is discussed.

The set-up used is a Fizeau interferometer. The lasertube and the power supply were integrated and fully isolated from the vacuum atmosphere outside to prevent spontaneous electric discharges. A beam expander was also integrated with the lasertube and consisted of a negative lens, a microscope lens and a pin hole. All these elements were arranged to provide an optimally expanded laser beam in such a way that the entire cell house was illuminated with an approximately even intensity distribution. One side of the cell houses (away from the laser) was covered with a black lid to avoid internal reflections. The other side accommodated a positive lens with a focal distance equal to the distance to the beam expander, to provide a parallel beam of light. Within the cell house two semi-reflective mirrors (4 % mirrors) were positioned, one before and one after the metal cross containing the V-shaped containers. These mirrors could be adjusted in such a way that both of them were approximately orthogonally oriented to the beam. They were adjusted to provide an interference pattern of roughly ten lines per cm. This interference pattern could be recorded by the camera. A shutter was built into the laser system that could block the laser light. This shutter could be activated simultaneously with the lamps that were positioned above the containers in the cell house. In this way, either the lamps were on, or the laser was ‘on’. These lamps were used to illuminate tracer particles in the liquid. During the experiment a pre-programmed sequence ran that alternated 5 seconds of laser light with 5 seconds of white light. This sequence could be overrun by tele-command. Overruling the sequence was done only during the first two minutes of the experiment. The

frequency with which laser and tracer pictures were alternated was increased a little during this period. The images seen by the camera were transmitted to the scientific centre in Kiruna, where they were recorded on tape.

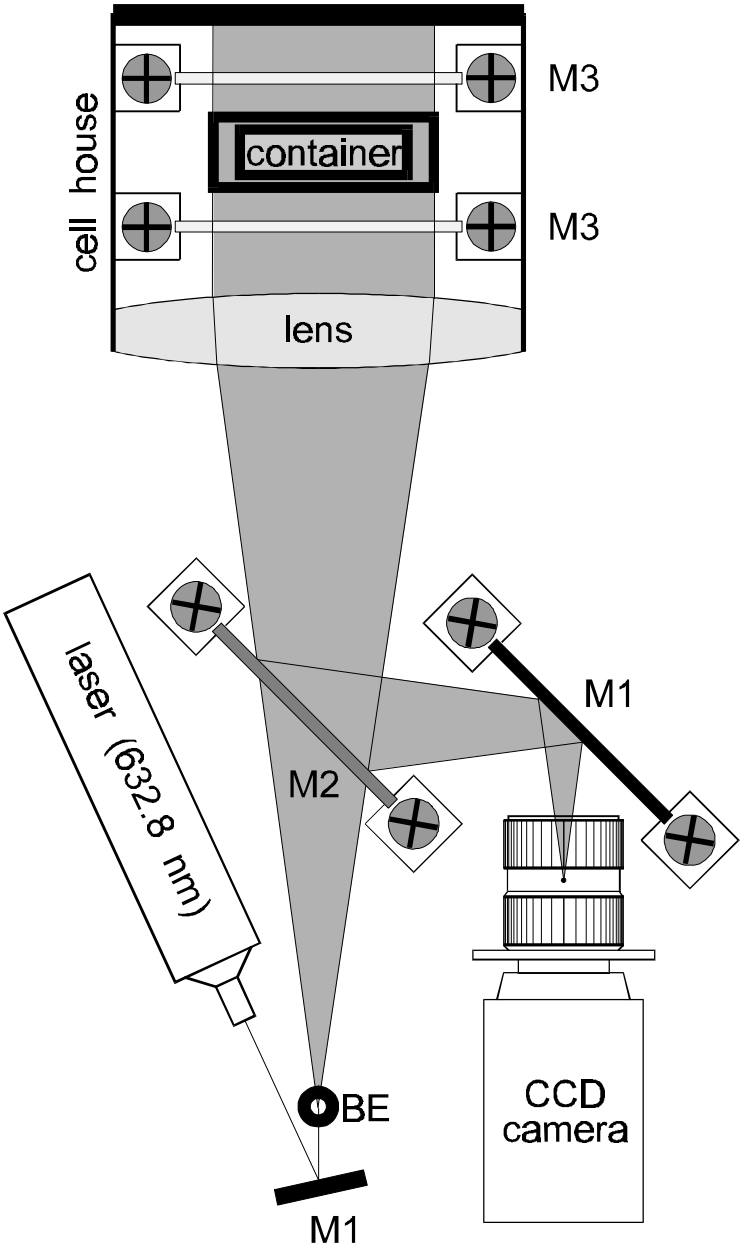

figure 4 *Sketch of the Fizeau interferometer set-up. BE = Beam Expander; M1 = mirror; M2 = semi-reflective mirror (80 % for 632.8 nm; 100 % for visible light); M3 = semi-reflective mirror (4 %)*

During the experiment, the camera would record either interferometry patterns or flow patterns. The lamps in the cell house illuminated the containers from the top (through the nets), showing tracers in the liquid. Tracer particles consisted of ceramic microballoons (Grace), coated (by precipitation reaction) with silver to improve their visibility and to increase their density. The particles were classified according to size (diameter between 100 and 150 μm)

and density (approximately the same as water). An example of a picture seen by the camera during laser illumination and during white light illumination can be seen in figures 5a and 5b. A cold mirror was located between the lamps and the container to avoid radiation heat effects (see figure 3).

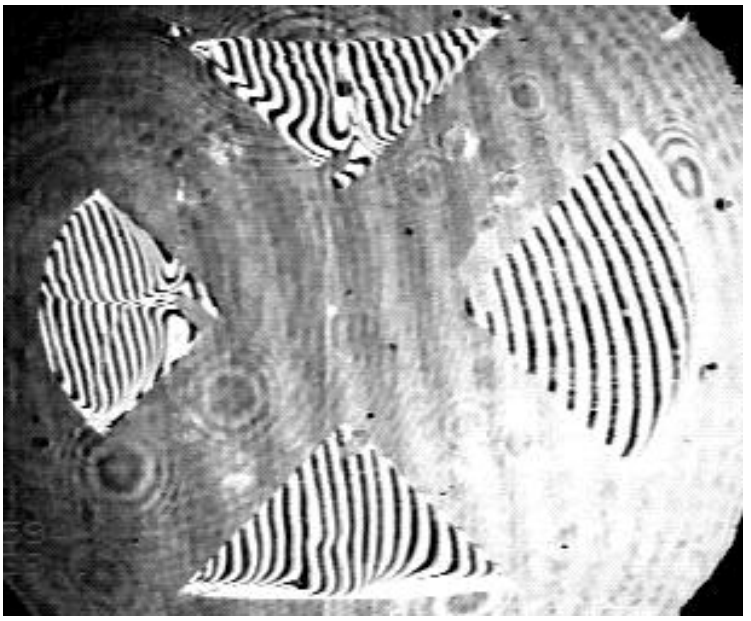

a

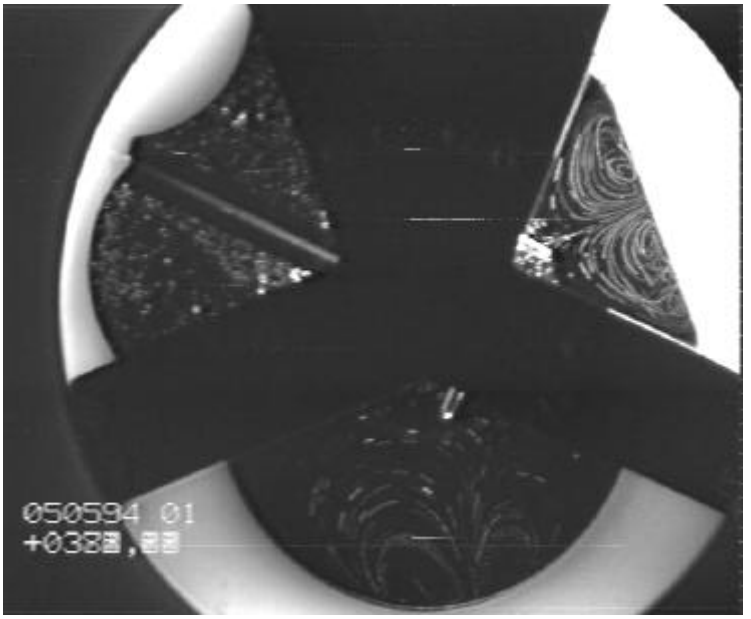

b

figure 5 *Video picture of the X cell house during interferometry after 294 seconds (a) and of the Y cell house during normal light between 265 and 290 seconds (b). Image b has been obtained by capturing video frames over a 15 seconds period.*

The liquid injection unit consisted of four syringes filled with liquid and tracers, a motor driving the syringe plungers, and a tubing system. Before the microgravity experiment, the syringes were filled with the appropriate amount of liquid to fill the containers exactly up to their rims. The error in the calibrated amount of liquid is an estimated 0.2 µl on a total amount of characteristically 0.25 ml. The injection unit containing the syringes could be inserted into the module shortly before launch. If the liquid was allowed to stand for too long in the syringe, pollution was anticipated. Syringes were sealed during take off and landing. The motor driving the plungers first opened the syringes before moving the plungers after microgravity had been achieved. Extensive tests with the hardware had been performed to establish the optimal amount of tracers in the syringes and the injection speed. The liquid used during the Texus-32 experiment was a 4.85 wt % acetone in water solution. The water was degassed to avoid the formation of air bubbles in the syringes before injection. Injection lasted 19 seconds, the real experiment time was 294 seconds and the time needed to reject the liquid from the containers lasted 21 seconds.

The experiment plates were internally thermostated until launch by a liquid circulation system that kept the plates on a constant temperature. The liquid was circulated through a tubing system that was connected via a ball valve to an external pump and an external thermostat. The valve on the rocket skin, connecting the inner circulation and the outer circulation system, was designed to close at the moment that the external tube was pulled out by the lift of the rocket. The whole system was designed to maintain a temperature equilibrium within the module, whereby temperature rise of the V-shaped containers should at no moment exceed 0.1 °C/min, temperature differences within the cell house should not exceed 0.1 °C and differences between cell house and air loop and between cell house and liquid injection system should not exceed 0.3 °C. Temperature requirements were based on two objectives:

- The intensity of macroscopic thermocapillary convection should not exceed approximately 1 % of the expected macroscopic solutal convection.
- Temperature gradients within the container should be small enough to keep refractive index variations due to unknown temperature variations within 5 % of the refractive index variations due to concentration variations.

Temperatures were measured with PT-100 elements on several locations: body of the cell houses, injection units, air pump and inside one of the quartz side walls of several containers (two in container 1, one in container 2, two in container 5 and one in container 7). PT-100 elements were located 0.5 cm from the top and 1.5 cm from the top (containers 1 and 5). A pressure sensor was present in each of the two cell houses.

Hardware for parabolic flight experiments

For the parabolic flight experiments, the experiment plate that was designed for the Maser 5 experiment was used, which contained the two cell houses and all the optic devices.

The cell houses were the same and the optical set-up was almost the same, albeit slightly less developed than the set-up used for Texus-32. The experiment plate was suspended from an experiment plate holder and the entire set-up was protected using a black metal cover. Syringes were kept outside the cover in order to inject the liquids manually (see figure 6). As microgravity time varied around 20 seconds, injection had to be quite fast. During each parabola, only one container could be experimented with. Liquid had to be rejected from the container before the end of microgravity time in order to repeat the experiment for the same container. In normal gravity, liquid would drop from the open side of the container, which would render it impossible to repeat an experiment for that particular container. Per flight of 31 parabolas, at least three experiments were conducted for each container. For container 1 and 7 also some experiments during normal and increased gravity levels were performed. This was possible by inserting the cross in the cell houses in such a way that these containers had their open sides up. For container 7, a nearly flat interface was created in these cases by withdrawing as much liquid as was necessary to get the liquid level below the left and the right upper corners.

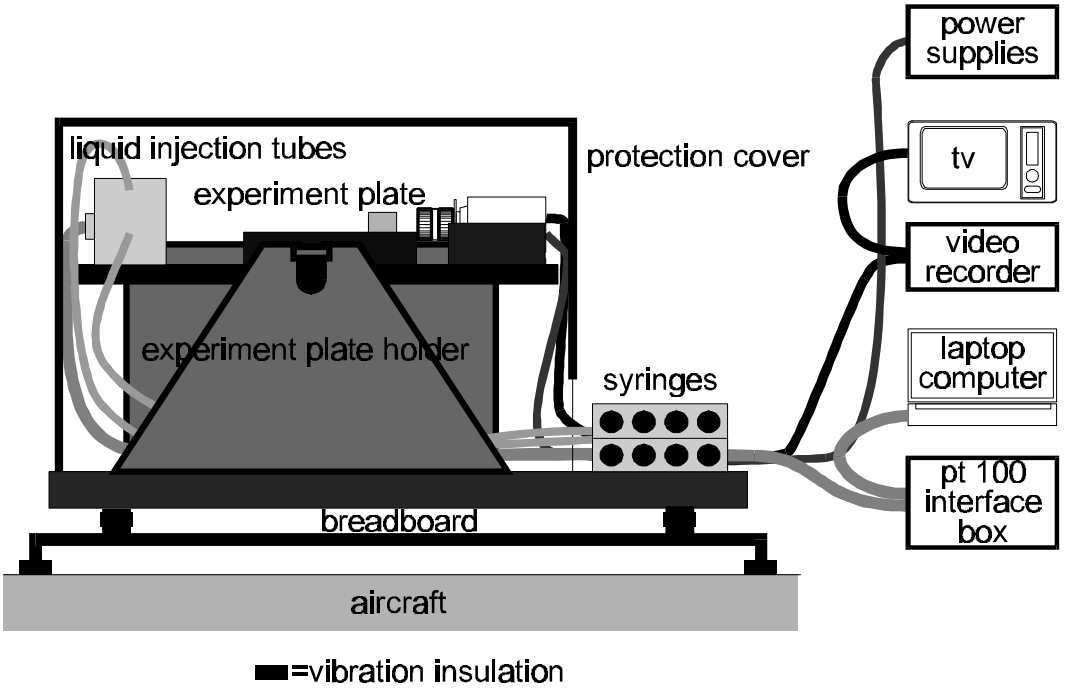

figure 6: Set-up for the parabolic flight experiments.

Description of experiments

In this subsection, all the different experiments and the circumstances under which they have been performed are summarised.

On Texus-32, experiments were performed under microgravity conditions using containers 1-8 and a 4.85 wt % acetone in water solution. Pressures were 1145 mbar in the X cell and 1000 mbar in the Y cell. With exactly the same equipment, ground reference experiments have been performed using the container 1 (4.83 wt % and 9.97 wt %) and container 5 (4.83 wt %). Using container 1, one reversed mass transfer experiment has been performed on this occasion as well, i.e. an absorption instead of a desorption experiment. This was done by saturating the air in the cell house with acetone and injecting water in the container. A small vessel with pure acetone was placed in the cell house to maintain the acetone concentration in the air at a high level. Another experiment was performed by injecting water in container 1 and thermostate the equipment to 15.3 °C. The resulting interference pattern was recorded and monitored while the equipment was slowly heated (in 80 minutes) to a temperature of 23.7 °C. This experiment was used to check the dependence of the interference pattern change on the refractive index change.

Using the same hardware, many tests have been performed prior to the Texus experiment and after the parabolic flight experiments. Usually, the hardware was modified slightly from the exact Texus-32 configuration (no deldrin pieces to create a well-defined air space, different injection speeds, different acetone concentrations etc.). Where appropriate, some of these tests are referred to, to illustrate a point. However, since the circumstances were not strictly defined in these cases, no quantitative importance can be attributed to these tests.

During the parabolic flights, experiments were performed using containers 1-8 under 10^{-2} g conditions. As described in the previous section, some experiments were also performed under 1 and 1.8 g conditions, using container 1 and 7. Liquid concentrations were varying around 5 wt % acetone in water.

2.3 Interferometry

The use of interferometry to obtain information about two-dimensional temperature or concentration fields is not new. Various papers can be found in literature, in which concentration or temperature fields are measured qualitatively (e.g. [5, 6, 7, 8 and references therein]. Sometimes, interferograms were used to obtain one-dimensional concentration profiles (e.g. [9, 10, 11]). Less papers exist in which a complete quantitative reconstruction of a two-dimensional refractive index field was performed (e.g. [12]). In the latter case, in which a Mach-Zehnder phase shift interferometer was used, the reference beam and the measuring beam had parallel wave fronts, in which case the occurrence of fringes can be related directly to gradients in refractive index in the measured sample. Here, a Fizeau interferometer was used to obtain a two-dimensional refractive index field in the V-shaped containers with the objective

to reconstruct a concentration map from these refractive index fields. In this section, the principle of the interferometer is discussed and the procedure used to turn the interference patterns into concentration maps outlined.

The Fizeau interferometer is depicted in figure 4. To understand the principle of interference, a close-up of the cross-section of the cell house is depicted in figure 7.

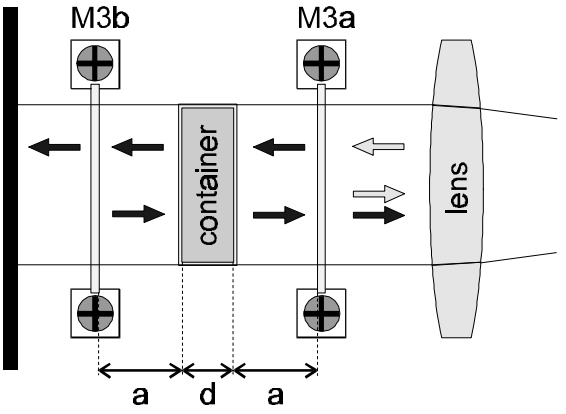

figure 7 Schematic cross section through the cell house, showing the light paths of beam 1 (grey arrow) and 2 (black arrow). M3 = semi-reflective mirror (4 %). See text for explanation.

Coherent, monochromatic, non-divergent, uniformly polarised light of the laser passes through the lens into the cell house. Here, the light first passes mirror M3a, where 4% of the light is reflected (beam 1). The light that is passing through this mirror (beam 2) passes through the container, reflects (partly) on mirror M3b, (largely) passes mirror M3a and interferes there with the originally reflected beam 1. The varying electric field **E** [V/m] of an electromagnetic wave in a lightbeam i can be described as a function of the co-ordinate of displacement z and time t as [13]:

$$\mathbf{E}_i(z,t) = E_{0i}\sin(\omega t + \alpha_i) \qquad (1)$$

$$\omega = 2\pi\nu = 2\pi\frac{v}{\lambda} \qquad (2)$$

$$\alpha_i = -(kz + \varepsilon)_i \qquad (3)$$

In these equations, ω is the angular velocity, α is the phase angle, λ is the wave length, k is the propagation number, ε is the initial phase, v is the speed of the light beam, ν is the frequency and E_{0i} is the amplitude of wave i. The irradiance I [W/m^2] is the time-averaged energy-flux per unit area generated by the light wave. In a homogeneous, isotropic, dielectric medium, the irradiance equals:

$$I_i = \left(\frac{ev}{2}\right)E_{0i}^2 \qquad (4)$$

In this equation, e is the dielectric constant. It can be derived [13] that two beams of light, 1 and 2, having equal velocities and being superposed on each other, generate a total irradiance equal to:

$$I = \left(\frac{ev}{2}\right)\left[E_{01}^2 + E_{02}^2 + 2E_{01}E_{02}\cos(\alpha_2 - \alpha_1)\right] \quad (5)$$

The extra term $2E_{01}E_{02}\cos(\alpha_2 - \alpha_1)$ in this equation is resulting from the interference of the two waves. The phase difference $\delta = (\alpha_2 - \alpha_1)$ is the important parameter that decides whether the interference is maximal (constructive interference), i.e. $\delta = \pm 2\pi, \pm 4\pi,...$, or minimal (destructive interference), i.e. $\delta = \pm \pi, \pm 3\pi,...$. The light and dark zones in the interference pattern that can be seen by an observer or camera, when placed in the right position, are the interference fringes (see e.g. figure 5a). The best interference patterns (most contrast) are obtained when the amplitudes of both waves are equal. Since the initial phases of the two waves are equal, the phase difference can be written in the following form:

$$\frac{\delta}{2\pi} = \frac{1}{\lambda_0}\int d(nz) \quad (6)$$

$$n = \frac{v_v}{v} \quad (7)$$

The term $\delta/2\pi$ is called the Optical Path Difference (O.P.D.), n is the refractive index and v_v is the speed of light in vacuum. From figure 7 and the assumption that the refractive index of the liquid in the container is no function of the z-co-ordinate, one can write:

$$O.P.D. = \frac{2}{\lambda_0}\left(2n_a a + n_{liquid} d\right) \quad (8)$$

In this equation, the term $2n_a a$ is the integrated product of path length and refractive index outside the liquid (including air and quartz wall). If refractive index values are equal across the area of the container, and the mirrors M3a and M3b would be exactly parallel, a uniform irradiance would result across the whole container and no fringes would be seen. By slightly tilting the mirrors with respect to each other, the optical path difference is varied across the entire area of the container.

In the rest of this chapter it is assumed that the term $2n_a a$ is not changing during the course of an experiment. This approach is justified, since the refractive index of air is only slightly dependent on the acetone concentration in the air (refractive index of the liquid is much more dependent on concentration), and refractive indices of quartz and glass are much less dependent on temperature than that of water. Therefore, changes in time in the O.P.D. values observed across the container can be attributed entirely to changes in concentration and temperature of the liquid. The refractive index at the start of the experiment n^0 is assumed to be known and constant across the container. By subtracting the O.P.D. values at each position x, y from the O.P.D. values at zero time, one obtains an ΔO.P.D. map, which can be changed into a refractive index map by the following relationship:

$$\Delta O.P.D^{t}_{x,y} = \frac{2d}{\lambda_0}\left(n^{t}_{x,y} - n^{0}\right) \qquad (9)$$

Data for refractive index as a function of concentration can be found in handbooks, but not for light with a wavelength of 623.8 nm. The following relationship for the refractive index increment dn/dc of an acetone-water solution at 20 °C was determined using a Jena interferometer:

$$\left(\frac{dn}{dc}\right) = 9.3\ 10^{-4}\ [wt\%^{-1}] \qquad (10)$$

The relation is valid between 4 and 6 wt %. This relationship is assumed to hold also for other temperatures used in the experiments, which were all close to 20 °C. An averaged value of dn/dT in the experimental range was interpolated from data in literature [14].

$$\left(\frac{dn}{dT}\right) = -8.8\ 10^{-5}\ [K^{-1}] \qquad (11)$$

In this chapter, ΔO.P.D. maps are presented rather than concentration maps. This is done, because slight temperature changes have also occurred during some of the experiments. A positive ΔO.P.D. value in a ΔO.P.D. map is chosen to relate to a refractive index that is lower than the original refractive index. Consequently, the higher a ΔO.P.D. value is, the lower the acetone concentration or the higher the temperature is (or a combination of both). From equations 9, 10 and 11 one can derive:

$$\left(\frac{\Delta c}{\Delta O.P.D.}\right) = -0.068\,[wt\%] \qquad \text{(containers 1-4, 6-8)} \qquad (12)$$

$$\left(\frac{\Delta c}{\Delta O.P.D.}\right) = -0.034\,[wt\%] \qquad \text{(container 5)} \qquad (13)$$

$$\left(\frac{\Delta T}{\Delta O.P.D.}\right) = 0.72\,[K] \qquad \text{(containers 1-4, 6-8)} \qquad (14)$$

$$\left(\frac{\Delta T}{\Delta O.P.D.}\right) = 0.36\,[K] \qquad \text{(container 5)} \qquad (15)$$

ΔO.P.D. maps were created along the following lines.

1. A video image of an interferogram was captured using a framegrabber (Imaging Technology PCVision Plus) and framegrabber software (TIM 3.3, Difa). The frame grabbing software was used subsequently to enlarge the picture, enhance its contrast and single out that part of the picture that needed examination (usually a container). (All non-relevant pixels in the digital picture were assigned a pixel value 0 (corresponding to black).) The final picture was recorded on tape. Macros were defined to ensure that all pictures concerning the same container were enlarged and positioned in the same way in the final picture.
2. These pictures were fed to a framegrabber connected to the optical imaging software Wisp2 (version 4.35, WYKO corporation), kindly made available by ESTEC. This program was able to digitise the fringes in the picture, i.e. lines were drawn using points in the middle of the white fringes. Some manual editing was usually necessary to correct faulty interpretation of the software.
3. In the area of interest, the program interpolated the lines using linear interpolation. From the resulting equations, the program could create an O.P.D. map across the whole area of interest. The program could not extrapolate outside the area surrounded by the fringes located at the outer edges of the relevant area.
4. From this O.P.D. map, the reference O.P.D. map, corresponding to the situation at the start of the experiment, was subtracted. This resulted in a final ΔO.P.D. map. An example of an interferogram at the start of an experiment, an interferogram at a specific time after the start of the experiment, and the resulting ΔO.P.D. map can be seen in figure 10.

5 One point in the container was chosen as a reference point. In this point, it was established visually how much the fringes had shifted since the start of the experiment. All the O.P.D. values in the map were related to this point. For example, if in the original ΔO.P.D. map the O.P.D. value was 0 in the reference point, but during the experiment the fringes had shifted two white-line-to-white-line-distances in this point, 2 was added to all the O.P.D. values to obtain the final ΔO.P.D. map.

This procedure had some drawbacks, apart from it being laborious:

- The program could either digitise and interpolate horizontal or vertical fringes. In the linear interpolation mode, a horizontal fringe, which would in part of its digitised path be vertical, would cause an interpolation error. Real fringes are sometimes even circular, and in areas where this would occur occasionally, the digitised fringe had to be manually edited to an ‘average’ position. Other interpolation modes, which could handle this kind of fringes (like Zernike polynomials), smoothed out all details that were relevant to this application.
- In case of large refractive index gradients, fringes could be too close to be distinguished individually. Fringes had to be digitised manually in these areas, but to the resulting O.P.D. maps only qualitative value can be attributed. Fringe density should not be more than 2-3 fringes/mm (area ± 20 mm long). I.e., gradients larger than 2-3 O.P.D./mm were impossible to measure quantitatively.

- Since no extrapolations were done outside the area that was bound by at least two fringes, the O.P.D. values close to the solid walls and the gas-liquid interface are not determined accurately.

All the results presented in this chapter should be interpreted keeping in mind the limitations described above.

As described in section 2.2, a test has been done to verify the quantitative reliability of the method, by slowly increasing the temperature of the entire cell house from 15.3 to 23.7 °C. Container 1 was filled with pure water. The other containers were empty. During the experiment, the fringes in the middle of container 1 slowly shifted to the left. In total, the fringe pattern shifted 9 fringe distances to the left. However, it was also noted that the line density in the entire cell house changed during the experiment. This has to be attributed to a slight tilt in the mirrors due to changing mechanical forces between the adjusting screws of the mirror and the body of the cell house. By examining points in the whole cell house the position of the tilting line was determined and by careful analysis of the interference pattern the total shift due to change in refractive index proved to be approximately 10.5; i.e. a change in O.P.D. value of 10.5 had occurred. According to equation 14, the O.P.D shift should have been 11.7. Given the uncertainty about the tilting effect, the agreement between these numbers is quite good. Knowing that the temperature change of the cell house during the experiments was quite small, the tilting effect is neglected in the rest of this chapter.

2.4 Results from the sounding rocket experiment

The sounding rocket experiment proved successful and all functions performed as designed, except for the following:

1. The anti-reflection coating on containers 3, 4, 6 and 7 was damaged partly. This produced a slight shift in the fringes from those areas in which the coating was not damaged to those areas in which it was (the anti-reflective properties were not lost). This damage was the result of the use of a liquid necessary for the coating of the Teflon layer on top of the containers. Only for container 7 this caused some minor problems in translating the fringe patterns to ΔO.P.D. maps.
2. One of the check valves on the rocket skin, connecting the cooling loop inside the module to the thermostat on the launch platform, did not close when the rocket was launched. Most of the cooling liquid escaped during launch and the remaining liquid evaporated when subjected to a vacuum atmosphere. This led to a decrease of temperature on the experiment plates. Although temperature drops on the injection units were most severe after injection, the temperature of the plates already dropped a little before injection. Therefore, upon injection, the liquid was 0.1-0.25 °C cooler than the containers (for container 2 even 0.5 °C). Graphs showing temperatures of the various PT-100 elements and of the cell houses are presented in figure 8. The temperature

variations in time and place may account for part of the O.P.D. changes in some of the presented plots. During the experiments, temperatures in the bottom of the containers were a little higher (± 0.1 °C) than in the top of the containers. This may be attributed to loss of heat due to evaporation. Despite all these temperature differences, convection was a result of concentration gradients rather than temperature gradients, as the results demonstrate. This is also supported by the analysis of Sternling and Scriven [2] and calculations presented in section 5.4.3.

3. In several containers pollution manifested itself, despite rigorous and lengthy cleaning procedures. In these cases no or only partial flow patterns developed. These cases are discussed in a little more detail below. Although Marangoni convection is very sensitive to pollution (the Plateau-Marangoni-Gibbs effect, see for example the review by Sternling and Scriven [15], the more quantitative study by Berg and Acrivos [16] and chapter 1), the observed total absence of flow, caused by whatever pollution present, is very surprising, considering the cleaning effort employed. Lichtenbelt et al. experienced a similar absence of convection during their experiment on D1 [17, 18], which was also attributed to pollution. Also in their case, rigorous cleaning procedures were employed..

The results of the sounding rocket experiments are presented and discussed per container.

Container 1

In container 1, a two roll cell pattern was expected to develop, based on ground-based and parabolic flight experiments [3]. Due to a larger surface to volume ratio in the corners, acetone depletes faster from the corners than from the middle of the container. This would cause a concentration gradient along the interface, the concentration being lower in the corners. The flow would be directed from the middle to the corners and two large roll cells would develop.

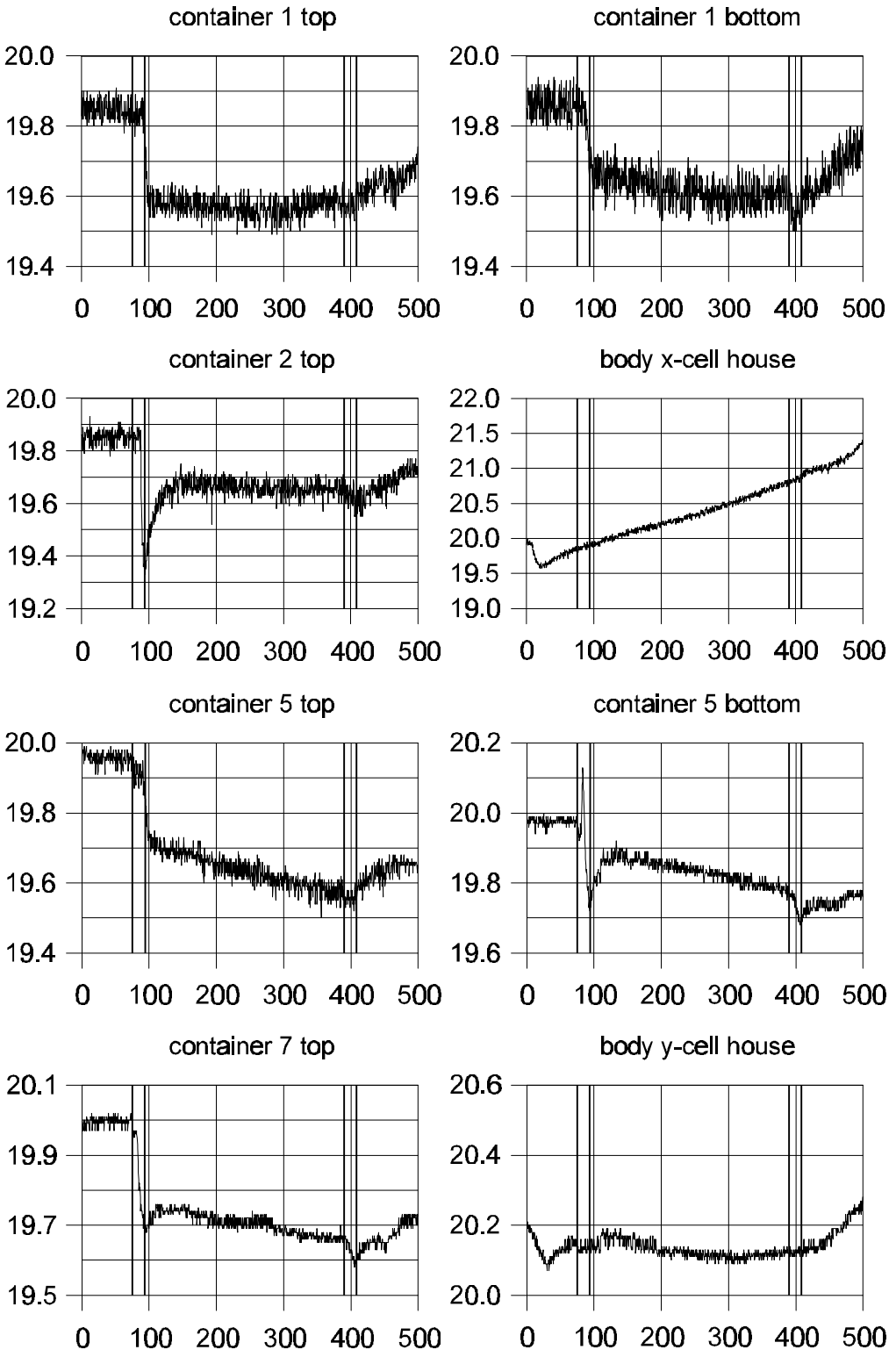

figure 8 *Temperatures during the Texus-32 experiment. Time is counted from lift-off. The vertical lines in the graphs mark the beginning and end of injection and rejection periods.*

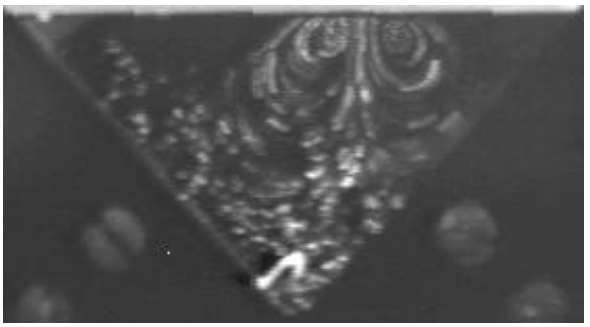

figure 9 Roll cells in container 1, between 63-66 seconds after the start of the experiment. Video frames have been added for 3 seconds.

However, this anticipated pattern of two large roll cells did not develop completely. In the beginning small roll cells (penetration depth 1-2 mm from the top) were seen. Very soon the flow was pulled outward by the developing concentration gradients, and two roll cells emerged with the middle of the roll cells being located right of the middle of the container (see figure 9). These roll cells moved slowly to the middle of the container and remained confined to the middle. Some pollution was presumably present in the corners as no convection was seen in the corners at all. The initial convection has swept all the surface active substances outward and created a clear patch in the middle. Straight fringes extended towards the interface on the cleared patch, while in the polluted corners the fringes were bent strongly close to the interface (see figure 10). This indicates that mass transfer was dominated by diffusion in the polluted areas, while convection was the principle mass transfer mode on the cleared patch. Velocities as well as the size of the clean area decreased in time, probably as a result of continuing absorption of surface active substances to the interface.

In the interfacial areas, in which diffusion was the main transfer mode, very large (penetration type) concentration gradients occurred, resulting in very large refractive index gradients. These areas can be recognised in the interferograms as grey areas. The light beam reflecting from the second mirror (M3b in figure 7) is deflected by the large refractive index gradient and only the reflection of beam 1 is observed by the camera (see also [5]).

The interferogram and the ΔO.P.D. map, corresponding to the situation 294 seconds after injection, are depicted in figure 10. The cleared patch and the polluted areas are easy to distinguish. It can also be seen that liquid with a higher acetone concentration has been transported from the bulk to the interface in the middle of the two roll cells (the middle of the cleared patch). Low concentration liquid has been transported into the bulk at the outer side of the cleared patch, explaining the curvy path of the isoconcentration lines. Contour lines of the flow are sketched in the interferogram.

Velocities at the clean interface are approximately 0.1 cm/s. Penetration depth of the final roll cells is 0.7 cm, while the middle of the roll cells is located 0.15 cm from the interface.

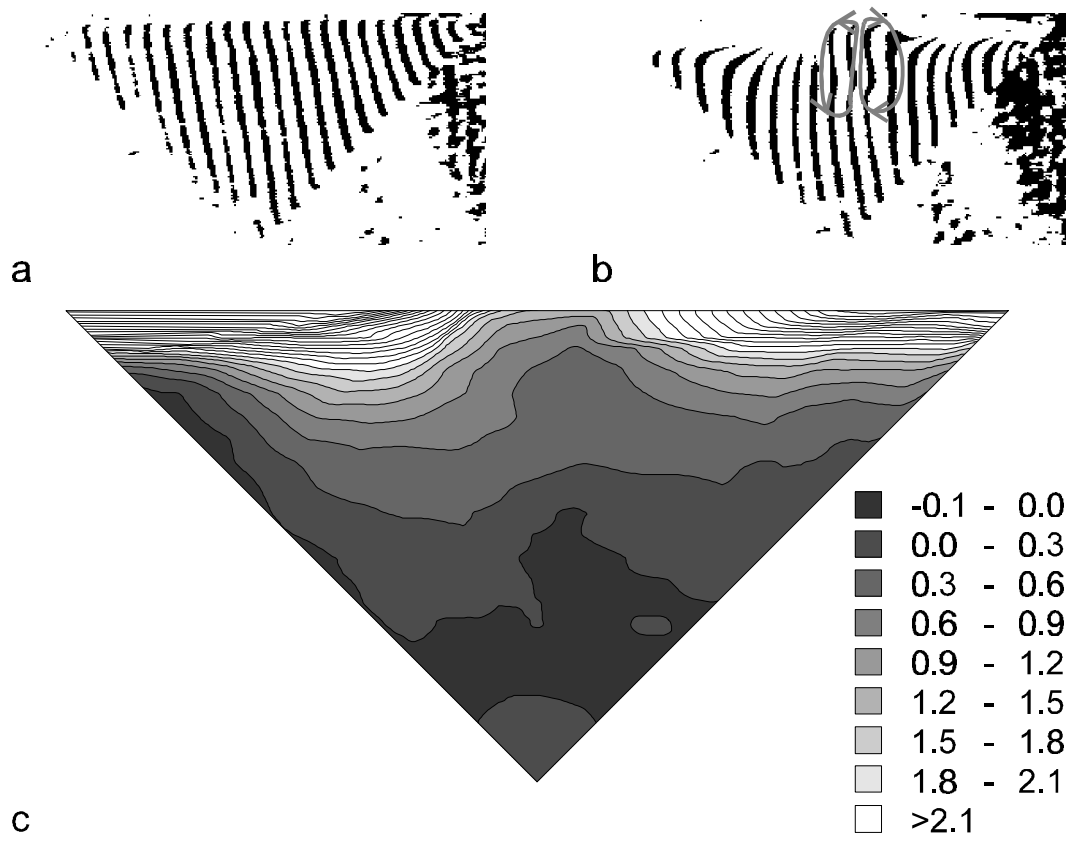

Figure 10 Interferogram of container 1 after 0 seconds (a) and 294 seconds (b), and the resulting DO.P.D. map (c).

Container 2

No convection at all was observed in container 2. Evidently, too much pollution was present in this container. Diffusion was the only mass transfer mode and this diffusion created the large refractive index gradients, also observed in container 1. In the interferograms, a grey layer (as discussed above) with a uniform thickness could be seen close to the interface. In figure 11, the interferometry pattern directly after injection, and the interferometry pattern after 294 seconds are depicted together with the ΔO.P.D. map after 294 seconds. In this map a distinct pattern can be seen that has remarkable resemblance to the injection pattern of the liquid. Cold liquid was injected and while liquid close to the walls and liquid in the 'island of low O.P.D.' were warmed up by the warmer container during injection, the liquid that was injected at the last moment before complete injection was comparatively cold. During the experiment this liquid has warmed up and this explains the large O.P.D. values in these places. Assuming the temperature in the liquid after 294 seconds is approximately uniform, the O.P.D. differences within the liquid at zero time are 0.6-0.7, corresponding to a temperature difference of 0.4-0.5 °C. This compares excellently to the temperature drop at the PT-100 located in container 2 (figure 8), which is 0.5 °C.

The penetration depth of the grey area into the liquid is approximately 1.5 mm. The penetration depth from penetration theory (= $\sqrt{\pi Dt}$) predicts this depth to be 1.1 mm, showing reasonable agreement with the experimental value ($D = 1.27\ 10^{-9}$ m^2/s [1]).

At rejection, sudden bursts of convection can be observed. Due to the rejection, concentration gradients parallel to the interface and thereby surface tension gradients were created suddenly which were large enough to overcome the stabilising influence of the Plateau-Marangoni-Gibbs effect.

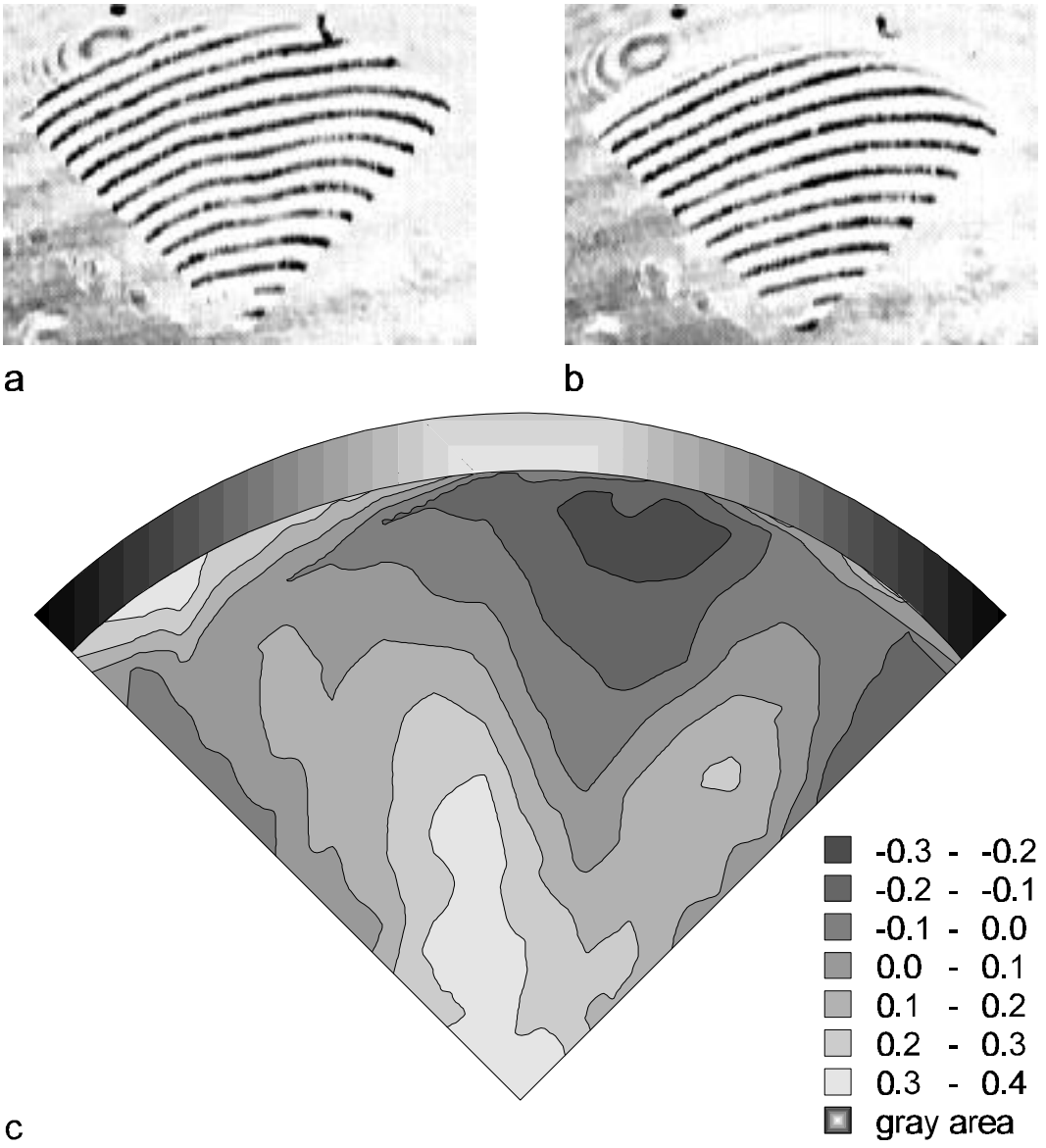

Figure 11 Interferogram of container 2 after 0 seconds (a) and 294 seconds (b), and the resulting DO.P.D. map (c).

Container 3

In container 3, an even larger difference in surface-to-volume ratio is present going from the centre of the container to the edges than in container 1. Therefore, a two roll cell pattern similar to the one described for container 1 is expected. The liquid in container 3, however, did not fill up completely to the corners, and was distributed a little unevenly over the corners as well, as can be seen in figure 12 and 13. Shortly after injection a large left-turning roll cell is occupying almost the entire container volume, while a very small right-turning roll cell can be seen in the upper right corner. The right-turning roll cell is growing in time, on the expense of the left-turning roll cell, until after approximately 3.5 minutes both roll cells occupy roughly half of the container volume. The right roll cell grows with a speed of 0.3 cm/min. The middle of the roll cells is located about 0.1 cm from the interface. At the interface, tracers are accelerated and follow a curvy trajectory. That is, tracers 'bump' away from the interface, return to the interface, accelerate and bump away again. Velocities at the interface are difficult to measure, but are roughly 0.4 cm/s. The roll cells penetrate deeply in the bulk of the container. In the final ΔO.P.D. map (figure 13b), it can be seen that only the concentration in the bottom of the container has hardly been influenced by the convection. Low concentration liquid is transported along the side walls into the bulk where it mixes with the high concentration bulk liquid. A flow of relatively high concentration liquid is directed to the interface at the division line between the roll cells.

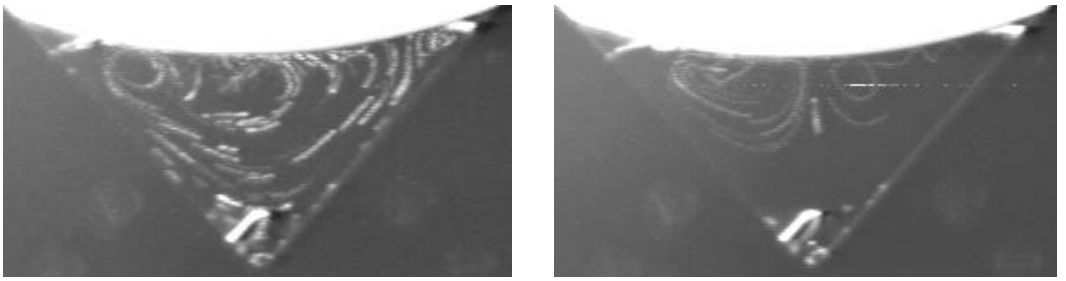

Figure 12 Video images of container 3 between 17-20 seconds (a) and 265-290 seconds (b). Frames have been added for 4 and 15 seconds, respectively. In the left figure (a) a very small roll cell can be seen in the upper right corner. Towards the end of the experiment two equally large roll cells have formed (b).

Initially, the right roll cell is smaller, and therefore the influence of convection on the concentration in this part of the container is relatively large. In the ΔO.P.D. map corresponding to the situation 69 seconds after injection (figure 13a), this can be seen clearly, as the concentration (O.P.D.) is lower (higher) in the right roll cell. During the entire experiment time, small roll cells, penetrating roughly 1.5 mm, can be seen appearing and disappearing, superposed on the macroscopic roll cells. Shortly after the start of the experiment areas of relatively low concentration can be seen at a depth of 1.5 mm, corresponding to this penetration depth.

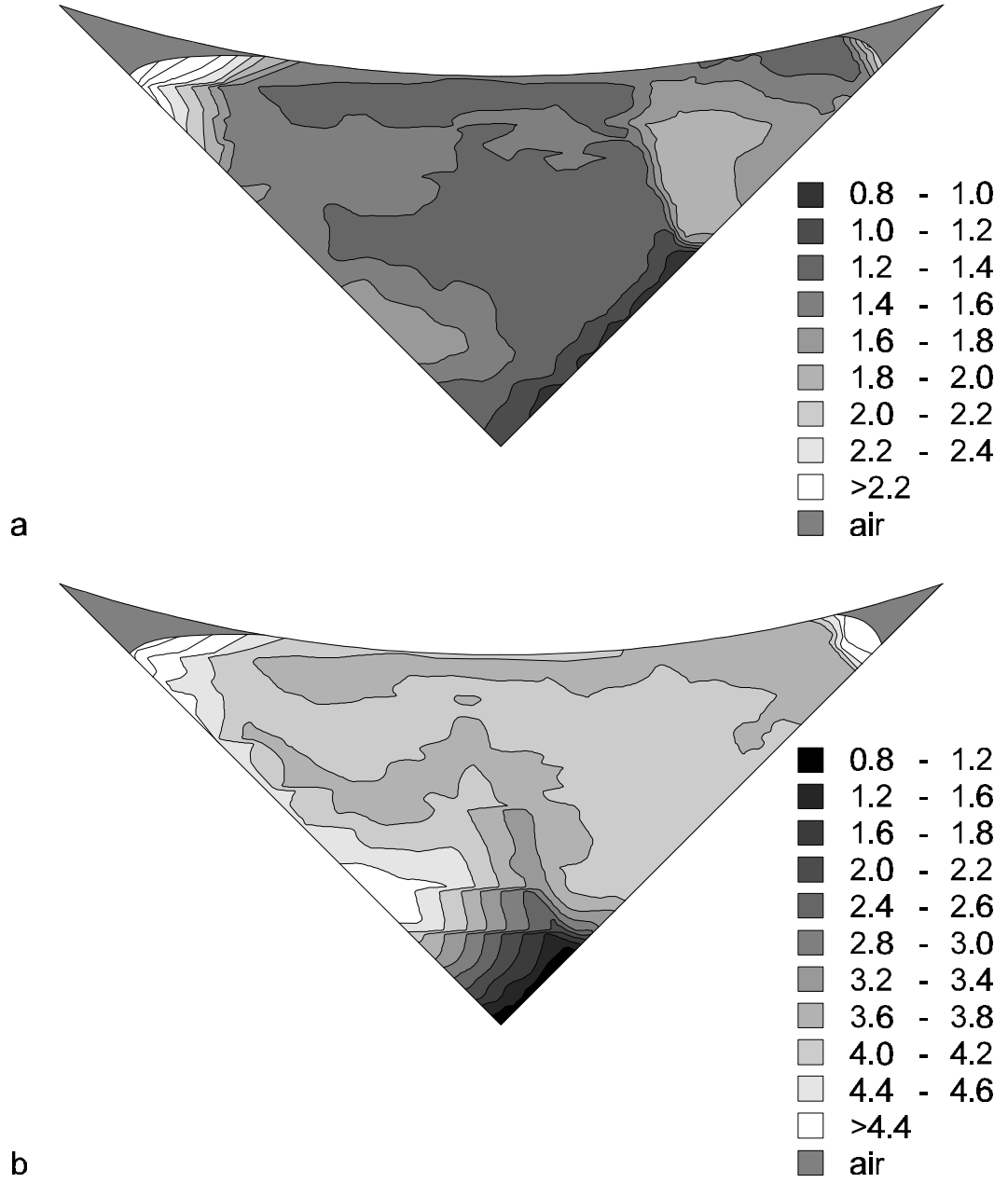

Figure 13 DO.P.D. map of container 3 after 69 seconds (a) and 294 seconds (b).

The initial size of the left-turning roll cell can be explained by the concentration distribution at the interface. In the interferograms it can be seen (not shown in the figures) that a little pollution is present in the left corner and that shortly after injection the O.P.D. values change much more in the left corner than in the right corner. This leads to a concentration profile along the interface, in which the maximum is located very close to the right corner. Whether only the different liquid-solid-gas contact angles in the left and right corner, or also an uneven distribution of traces of pollution play an important role in this, can not be assessed from the video pictures. Later, the small roll cell grows on the expense of the larger roll cell.

This can be explained primarily with the concentration distribution. Since the overall concentration in the smaller roll cell is somewhat smaller than in the larger roll cell, due to its faster depletion, the concentration differences in the smaller roll cell are larger, and, due to its size, the interfacial concentration gradients even larger. This results in a larger interfacial force on a smaller liquid volume. The smaller roll cell therefore turns faster than the larger roll cell and a net force towards the larger roll cell results. The dividing line between the roll cells shifts away towards the roll cell with the smaller vorticity.

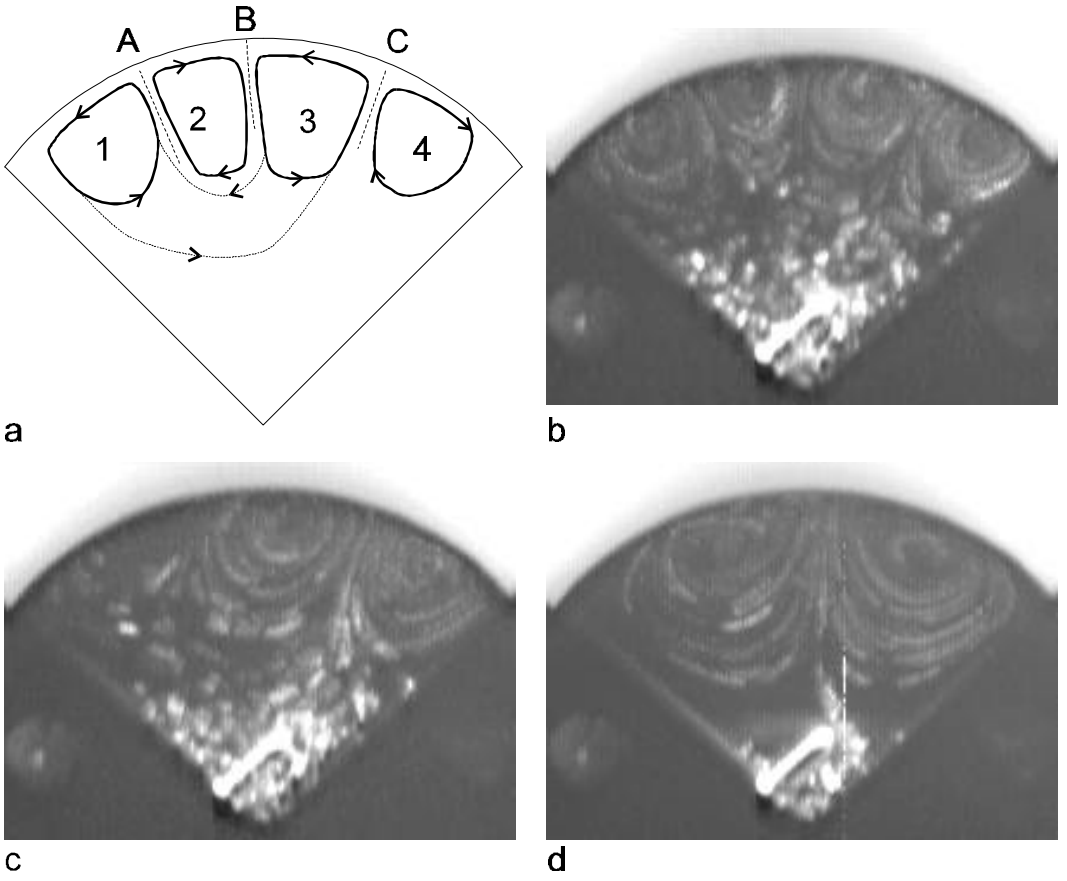

figure 14 *Roll cell pattern in container 4 between 17-20 seconds (a and b), between 32-35 seconds (c) and between 265-290 seconds (d). Video frames have been added for 3, 3 and 15 seconds, respectively. The dotted lines in figure a indicate how roll cells 1 and 3 merge, which results in the disappearance of roll cell 2 (see text).*

Container 4

Container 4 was designed to have a slightly larger surface to volume ratio in the middle than in the corners (the distance between the corner of the V to the interface is 15 mm along the centreline of the container, and it is 14.1 mm along the side walls). It was anticipated that this could lead to two large roll cells turning exactly the other way around as in container 1, 3, 5 or 6. However, the experiment showed quite different results.

Directly after injection, convection was observed with a penetration depth of 1-1.5 mm from the interface. No separate rolls can be observed until 5 seconds after injection. After 11 seconds, however, four roll cells can be distinguished (see figure 14a/b). The centre of the roll cells is then 0.13 cm from the interface and they penetrate roughly 0.6 cm. An estimate for the interface velocity is 0.3 cm/s. The velocity in between rolls to or from the interface is approximately 0.15 cm/s. After 22 seconds, the middle line between roll cell 2 and 3 (i.e. B) starts to shift to the left with an average velocity of 0.08 cm/s. After 35 seconds, roll cell 2 disappears and roll cell 1 and 3 merge into one large roll cell, turning left. The right roll cell then starts to grow till both roll cells are approximately equally large.

In the final situation two large roll cells exist. These rolls transport liquid with a low acetone concentration from the corners of the container into the bulk where it mixes with high concentration liquid from the bulk. Between the roll cells liquid with a relatively high concentration is transported to the interface. ΔO.P.D. maps showing the concentration distribution after 20, 40, 121 and 294 seconds are depicted in figure 15. An interferogram of container 4 after 294 seconds can be seen in figure 5a. The centre of the roll cells remains at a distance of 0.15 cm from the interface. Interface velocities are approximately 0.4 cm/s. The velocity in between the roll cells close to the interface is roughly 0.2 cm/s. Superposed on the two big roll cells, small roll cells can be observed at the interface.

The anticipated roll cell pattern of two rolls rotating the other way around than observed experimentally was not seen. This can be due to various effects. Firstly, the gradient in surface to volume ratio was very small, so the effect is easily diminished by other effects. Furthermore, liquid may not have filled up completely the container, but a slight over- or underfill is easily possible. Geometrical effects caused by the meniscus might have created concentration gradients that easily overshadow the aforementioned gradients. Pollution that absorbs near the solid-liquid contact line co-operates to the meniscus effect. An analysis by Dijkstra for transient Marangoni convection in a square container (with slippery side walls) shows that a two roll cell pattern with the left one rotating clockwise is more unstable [19]. A bifurcation study by the same author indicates that such a system is always unstable for higher Marangoni numbers [20]. This can be envisioned by realising that the rigid sidewall causes velocities away from the wall to be higher than at the wall. If a flow with high concentration is directed upwards along the wall, a spot with higher concentration is formed at the interface where the velocities are highest. At the interface close to the wall the concentration is lower, and a counter-rotating roll cell forms at the wall. Also, results presented in chapter 3 for a convex container confirm that a roll cell is not stable when the flow is directed downward at the side wall.

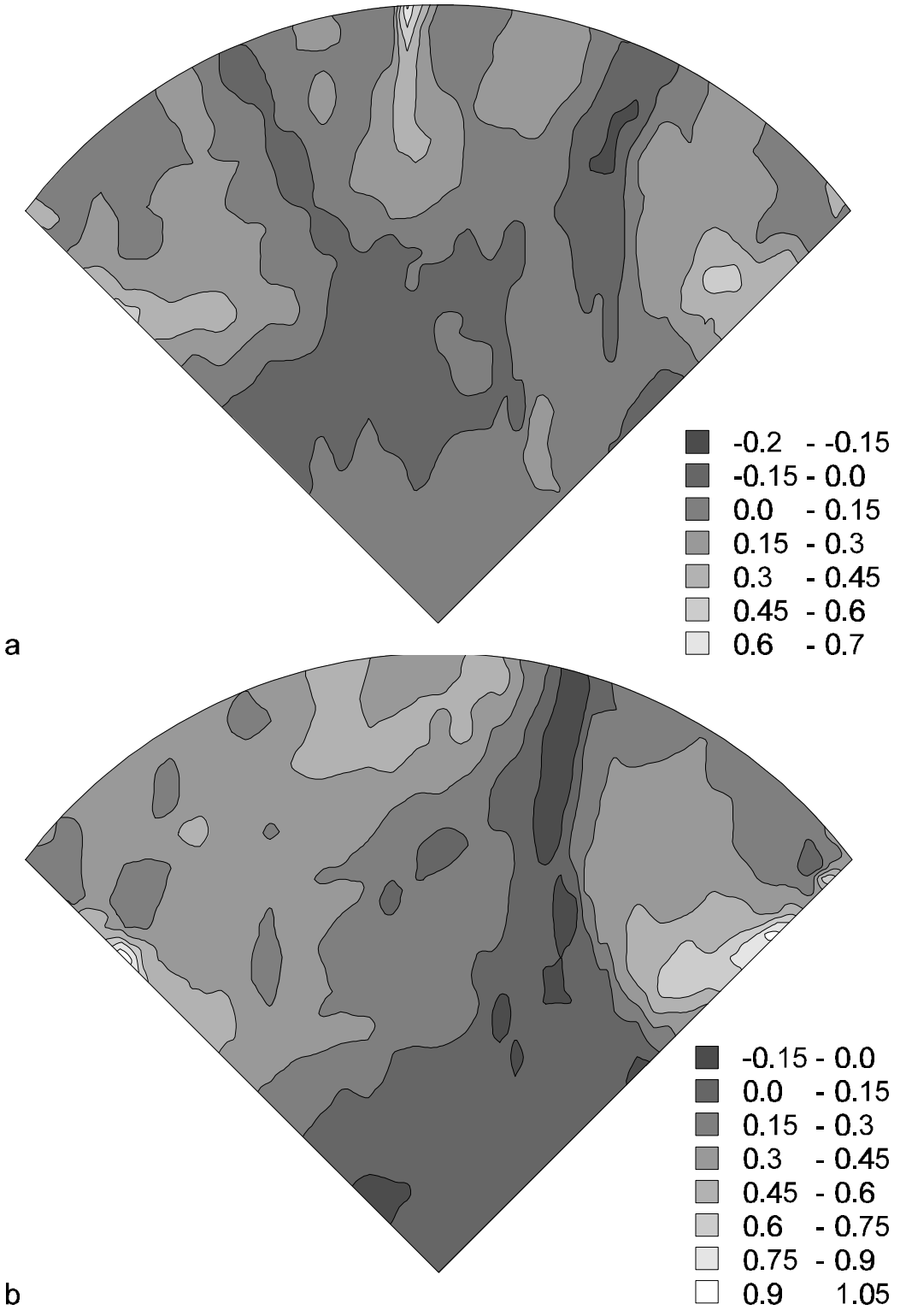

figure 15 DO.P.D. map of container 4 after 20 seconds (a), 40 seconds(b).

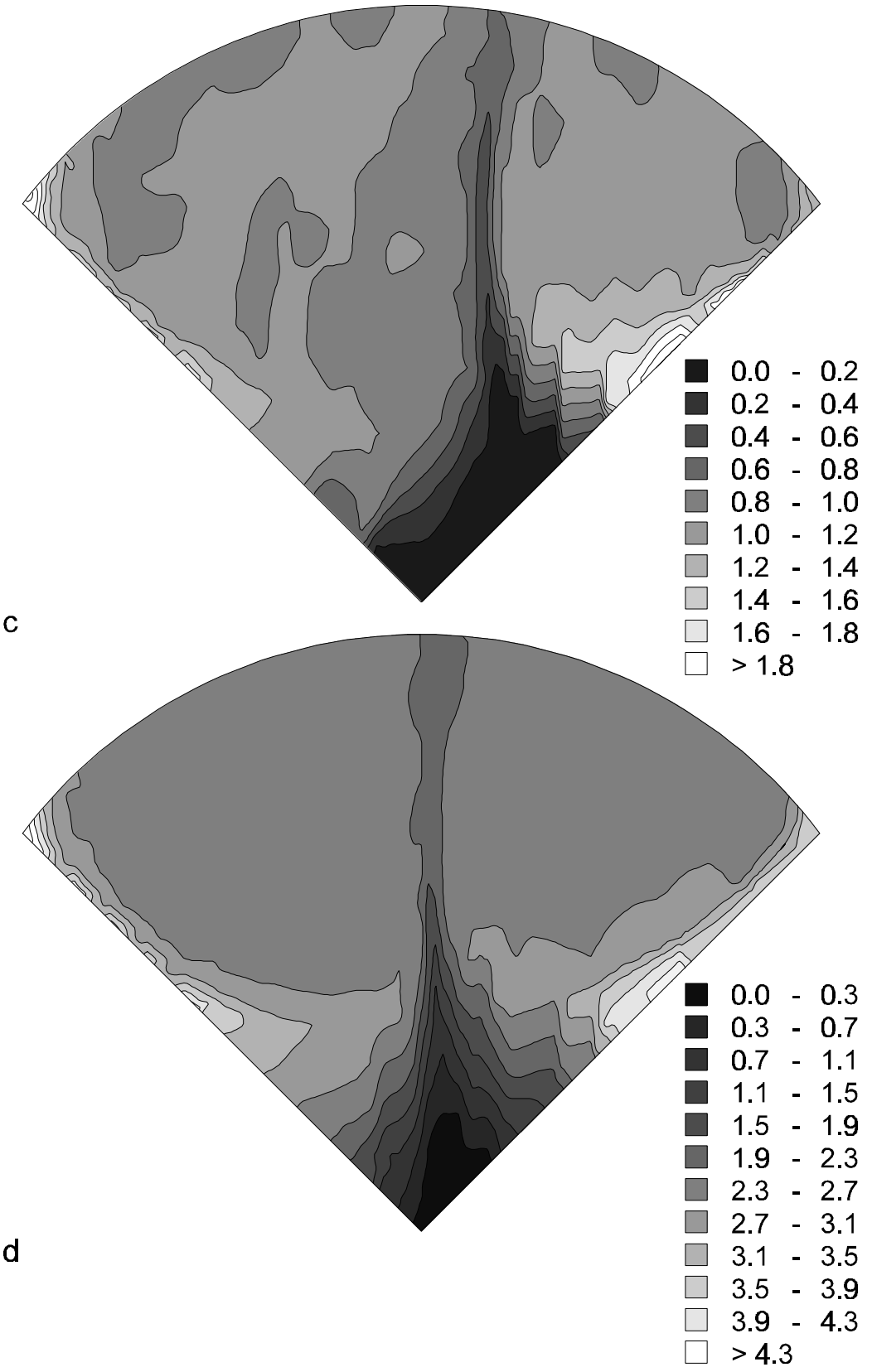

figure 15 DO.P.D. map of container 4 after 121 seconds (c), 294 seconds(d).

The observed pattern of four roll cells merging into two stable roll cells is only partly explainable from basic considerations. Initially, microconvection develops, since no large macroscopic gradients exist. The pattern in which this convection organises itself is determined by a balance of entropy production (minimisation of concentration gradients, minimisation of self-organisation) and enthalpy consumption (minimisation of viscous dissipation, minimisation of surface tension). It is impossible to predict a flow pattern based on qualitative observations. Pattern selection can be predicted theoretically by performing a bifurcation study and/or calculating the transient development of the Marangoni convection [21]. Without doing so here (however, see chapter 3), one can only conclude that a four roll cell pattern is energetically the most favourable situation for this geometry as long as the penetration of the roll cells in the bulk is not too high (this is confirmed theoretically for square containers by Dijkstra [19]). For larger times, the convection in the bulk influences the total pattern. If, in this case, roll cell 3 is slightly more intense than roll cell 2, roll cell 1 and 3 merge in the bulk (see the dotted lines in figure 14a). From then, the liquid coming to the surface in C has a higher concentration than the liquid in A. Velocities between B and C are therefore slightly larger than those between A and B. B starts moving to the left and roll cell 2 disappears. One could think that the width of the container (0.5 cm) also relates to the initial four roll cell pattern, as the overall dimensions of a roll cell is then roughly equal in any direction. However, the analysis in chapter 3 shows that also for a container with infinite width, a four roll cell pattern is the most stable for short times and a two roll cell pattern the most stable for long times.

Container 5

In container 5 the same roll cell pattern was anticipated as for container 1, but, due to its larger depth, some higher velocities were expected and a three-dimensional component might also be present. Container 5 did not fill up completely into the corners and a very small amount of impurity seemed to be present in the left corner. After 5 seconds, intensive (micro-) convection can be seen at the entire interface, but the general flow is already directed from the middle to the corners. Penetration of the flow (moving tracers) can be seen at a depth of 0.59 cm after 11 seconds. Penetration of impulse can be estimated from $\sqrt{\pi \nu t}$, ν being the kinematic viscosity (10^{-6} m^2/s), which excellently compares to the experimentally estimated penetration depth. Structured flow has started almost immediately, therefore.

Two large roll cells grow fast and occupy almost the entire volume of the container (see figure 16). Especially in the right roll cell a very intense small roll cell turning the same way as the large roll cell (to the right) is superposed on the flow very close to the edge of the container. This intense convection cell can not be seen in the left corner (presumably due to the pollution). The change in O.P.D. in the right roll cell is therefore also a little larger than in the left roll cell (see figure 17). Although no intense small roll cell can be seen in the left corner, in the left roll cell as well as in the right roll cell flow along the interface is not directed parallel to the interface going from the middle of the container to the corner. Tracers coming to the interface are swept outward parallel to the interface, slow down as they go into the bulk

(roughly 0.2 cm), and are accelerated again, in a way similar to roll cells observed by Linde et al. [22]. Apart from this, also a three dimensional component can often be seen. However, this is not exclusively valid for container 5, as also in the other containers three dimensional flow (spiralling tracers along the interface) can be seen.

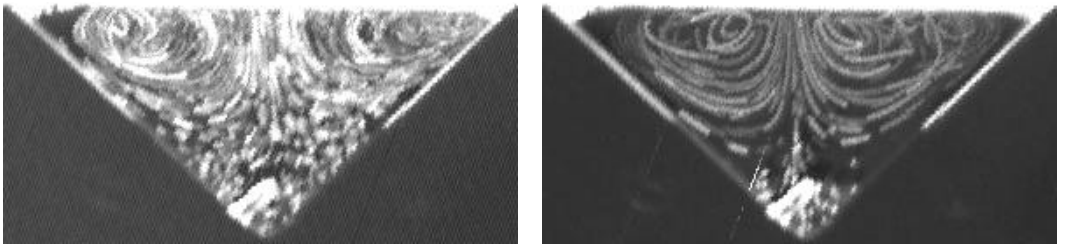

figure 16 Roll cell pattern in container 5 between 6-10 seconds (a) and between 265-290 seconds (b). Video frames have been added for 4 and 15 seconds, respectively.

Maximum flow velocities are roughly 0.5 cm/s at the interface and 0.25 cm/s in the middle of the container normal and close to the interface. The centre of the roll cell is located at a distance of roughly 1.5 mm from the interface. ΔO.P.D. maps are depicted in figure 17 after 69, 181 and 294 seconds. From these pictures it can be seen that the concentration distribution more or less keeps the same form, although the differences become larger. The flow, therefore, is very stable.

Container 6/8

In container 6 and 8 no flow was observed, probably due to pollution. The penetration depth of the 'grey area' in the interferogram after 294 seconds is roughly 0.12 cm and 0.14 cm respectively (theoretically 0.11 cm; see container 2). Like with container 2, the temperature of the liquid equilibrated during the experiment corresponding to an O.P.D change of 0.75 (0.5 °C) and 1.0 (0.7 °C), respectively. Upon rejection sudden bursts of flow were observed for both containers.

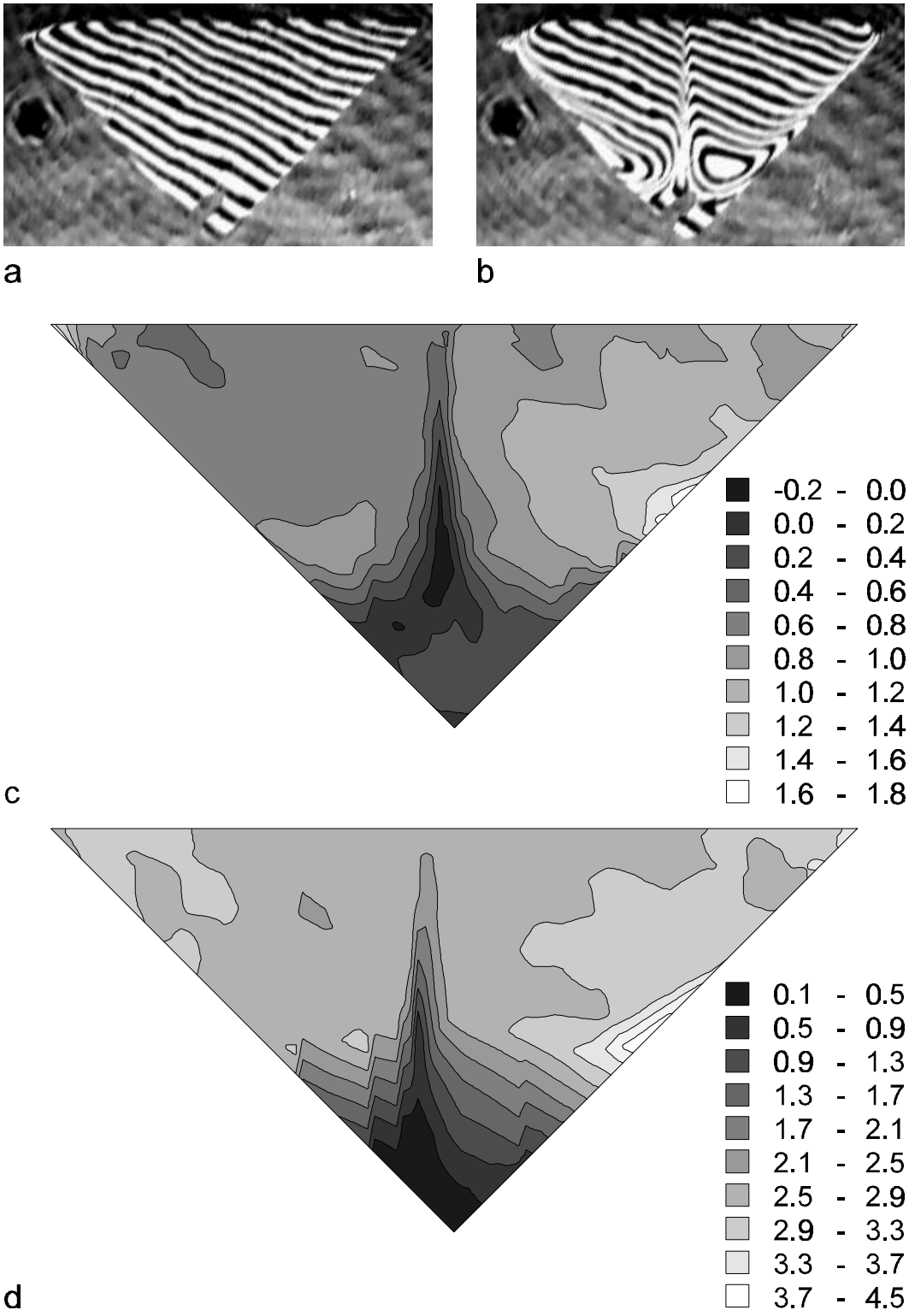

figure 17 Interferogram of container 5 after 0 seconds (a) and 294 seconds (b) and DO.P.D. map of container 5 after 69 seconds (c) and 181 seconds (d).

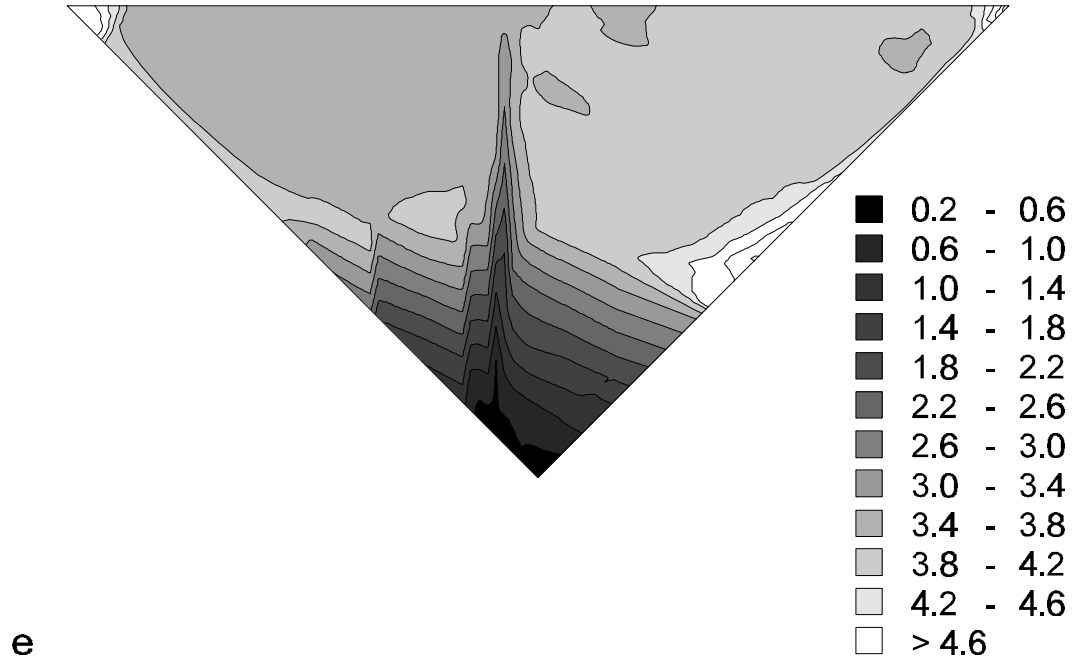

figure 17 DO.P.D. map of container 5 after 294 seconds (e).

Container 7

In container 7, like in container 2, microconvection was expected, since no macroscopic asymmetry with respect to the concentration field is present for this system. The results for container 7 are quite similar to those for container 4. After 5 seconds convection is observed at the interface (penetrating roughly 0.15 cm). No individual roll cells can be distinguished. In the outmost left corner pollution seems to be present as no convection is visible here. The flow penetrates 0.46 cm after 8 seconds, 0.62 cm after 14 seconds and 0.92 cm after 21 seconds. (This is the depth at which the interference fringes are slightly bent.) Penetration of impulse estimated with a penetration depth $\sqrt{\pi \nu t}$ should be 0.50, 0.66 and 0.81 respectively. Structured flow has started almost immediately, therefore. After 16 seconds four roll cells can be distinguished, analogous to container 4. Flow velocities are up to 0.5 cm/s at the interface and 0.2-0.25 cm/s normal to the interface at the lines separating the roll cells (both from and to the interface).

The roll cell pattern after 40 seconds is depicted in figure 18. In this figure some interferograms are also depicted that give a good insight in the flow development in container 7. After 95 seconds the separation line between roll cell 2 and 3 (i.e. A) starts to shift to the right (this is easily observable in the interferograms) with an average speed of roughly 0.1 mm/s. The separation line between roll cell 3 and 4 (i.e. B) remains roughly at the same place. Between 145 and 150 seconds A and B meet. Roll cell 2 has disappeared and roll cell 1 and 3 have merged. From the merging point an eddy separates with a lower concentration, moving the same way as the large roll cell (see figure 18d). This roll cell can also be distinguished as a

higher O.P.D. area in figure 19d. From the moment the four roll cells have disappeared, the convection in the right corner diminishes, which can also be seen in the interferograms. In both corners larger concentration gradients are present due to the absence of convection, i.e. due to the presence of pollution. Maximum velocities in the two roll cells are roughly the same as those in the four roll cell situation, although in one case a maximum interface velocity of 0.6 cm/s was observed. The centre of the roll cells is located at roughly 0.15 cm from the interface. Various ΔO.P.D. maps are depicted in figure 19. The flow development can nicely be recognised in these ΔO.P.D. maps.

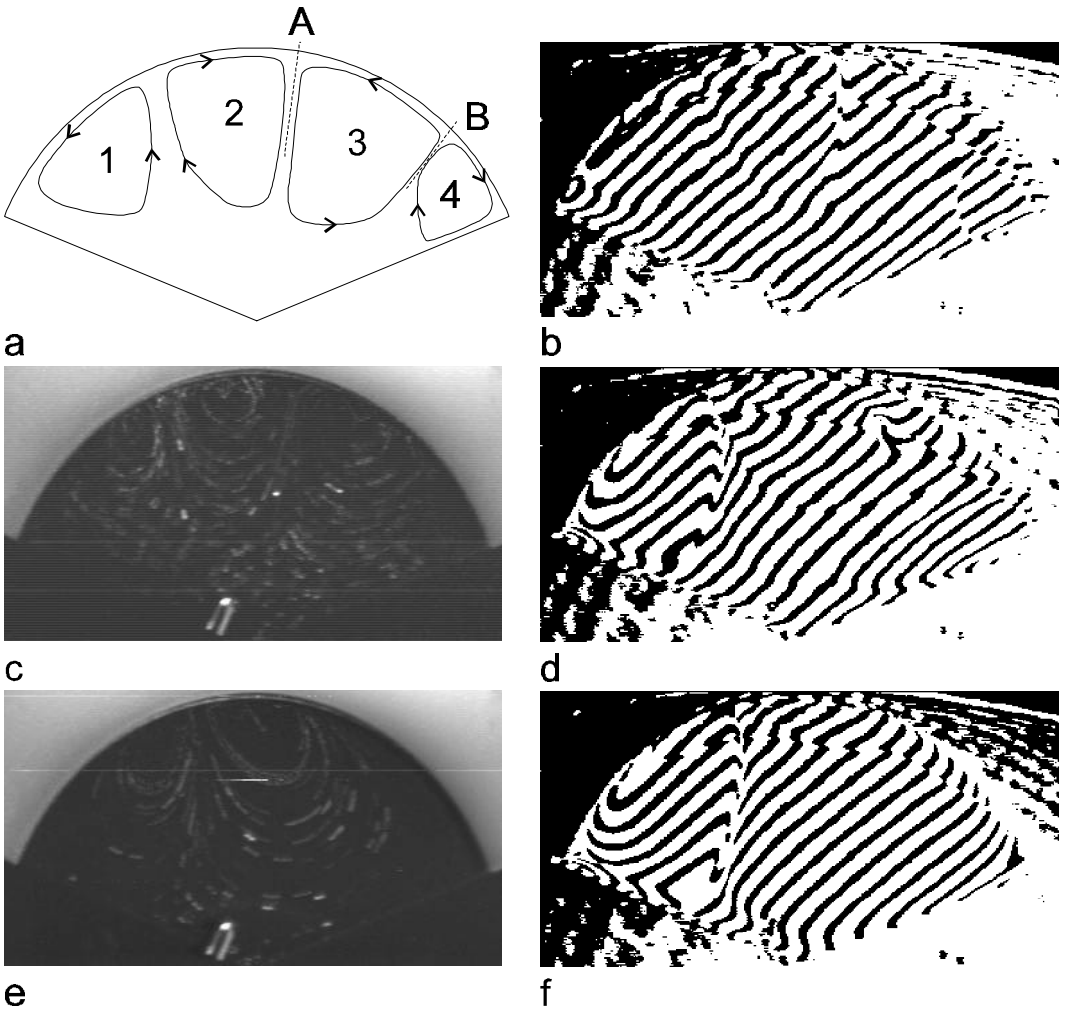

figure 18 *Roll cell pattern in container 7 after 40 seconds (a), 17-20 seconds (c) and 265-290 seconds (e). Video frames have been added for 3 (c) and 15 seconds (e). Interferogram of container 7 after 40 seconds (b), 151 seconds (d) and 294 seconds (f). Note the little eddy just right of the middle in figure d.*

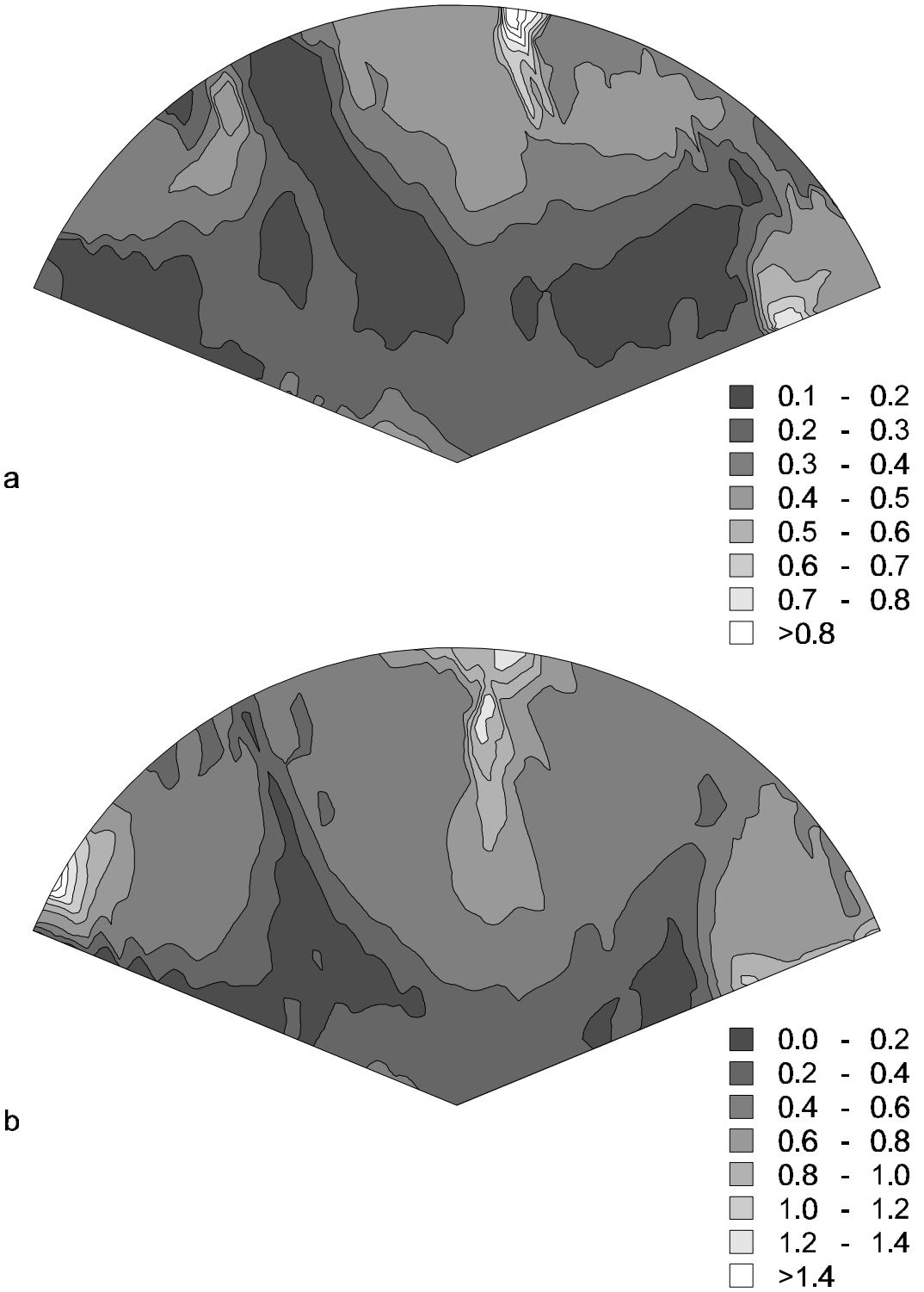

figure 19 DO.P.D. maps of container 7 after 27 seconds (a) and 69 seconds (b).

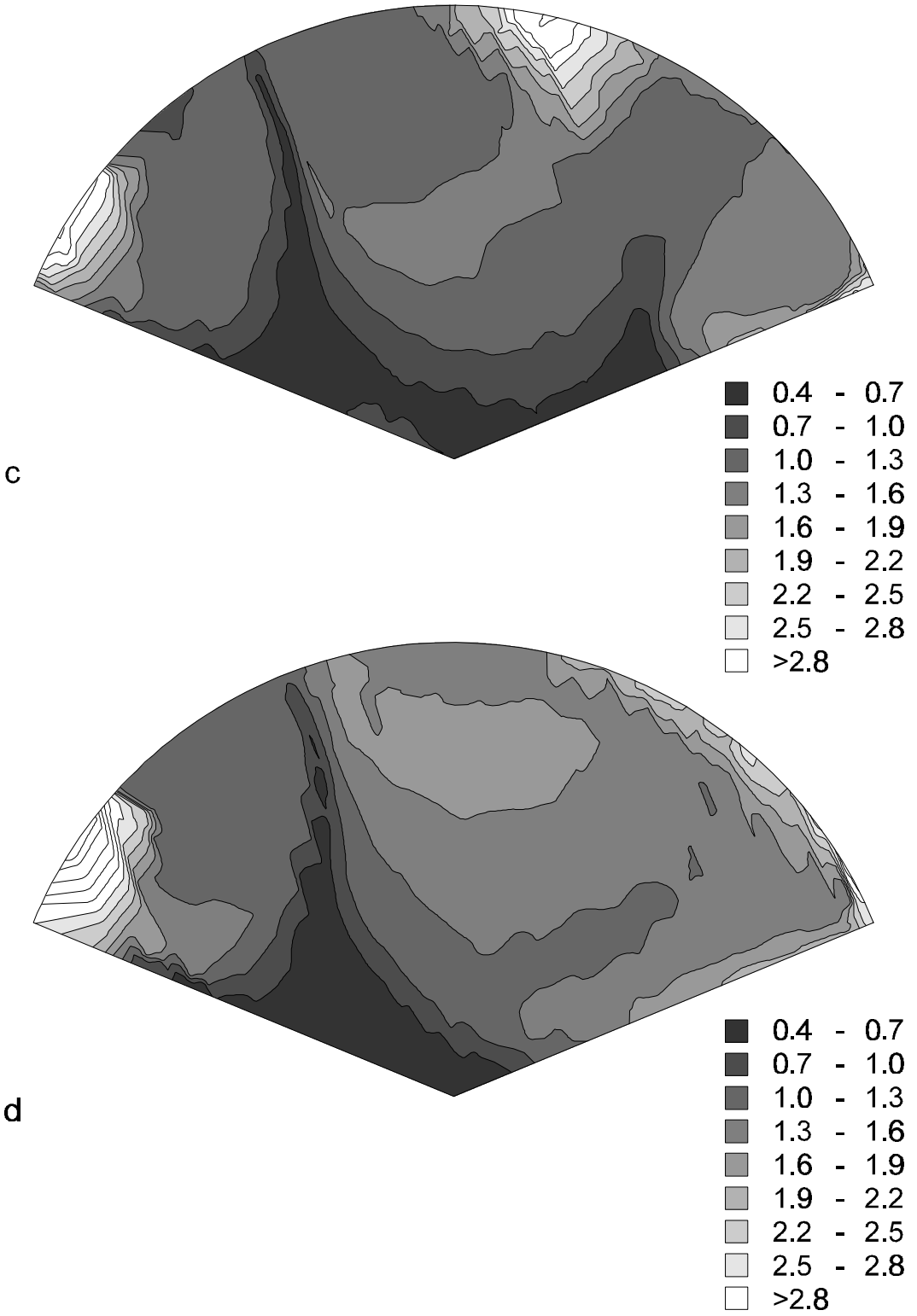

figure 19 DO.P.D. maps of container 7 after 121 seconds (c) and 181 seconds (d).

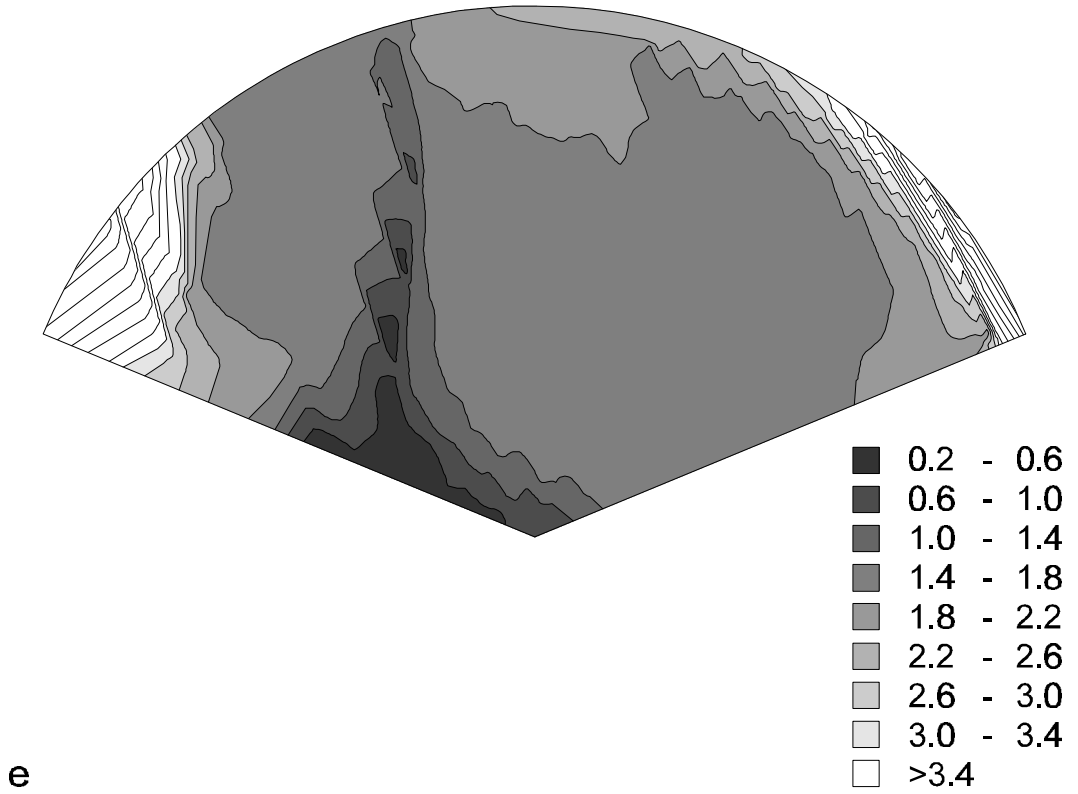

figure 19 DO.P.D. map of container 7 after 294 seconds (e).

An explanation for the flow development in this experiment can partly be given along the same lines as those for container 4. The longer lifetime of the four roll cell pattern can be explained by the different size of the containers (bulk flow exerts its influence on the flow pattern in a more spacious container in a later stage). The pollution in both corners probably also has had its influence on the streampattern. One might think the pollution creates the asymmetry in the concentration field, thereby favouring a two roll cell pattern. However, calculations on a 'clean' system (chapter 3) indicate that the two roll cell pattern is the most stable (energetically favourable) situation, even without pollution.

2.5 Results from various 1-g experiments

Reference experiment container 1 (4.83 wt %)

Directly after injection fringes at the interface bend. This bend corresponds to a decrease in concentration, and it moves slowly away from the interface. However, between the bend and the interface O.P.D. values are almost unchanged from the initial values. This phenomenon has also been observed with container 3 and 7 during microgravity and with countless other earth experiments. As the bend moves at a speed with which impulse penetrates (see section 2.4,

container 7), the most probable explanation for this is the almost immediate formation of a roll cell normal to the viewing plane. This roll cell takes low concentration liquid from the interface to a depth corresponding to the depth of the roll cell. Roll cells like the one described are also seen in the tracer pictures (not shown). The bend is most obvious till a depth of roughly 0.5 cm is reached, which is also the width of the container. After a short initial period, roll cells with their major velocity component in the viewing plane take over, which also explains why the bend disappears after a while. A clear example of a bend in the interferogram is depicted in figure 24 and resulting ΔO.P.D. maps are depicted in e.g. figures 21a and 25a.

For a short period between 5 and 20 seconds, the formation of four roll cells in an analogous way as seen with container 4 and 7 in microgravity can be observed. In the ΔO.P.D. maps this formation is very clear (figure 21b), but also tracers reveal this flow pattern, albeit less obvious (see figure 20). After 20 seconds, the two right turning roll cells have united and a two roll cell pattern emerges. The two roll cells remain stationary for the rest of the experiment. However, the flow pattern differs from the two cell roll pattern in container 5 in microgravity. The low concentration, high density, liquid that flows into the bulk along the solid boundaries penetrates deeply in the container and lowers the concentration in the bottom of the container. The presence of pollution in the corner causes more high density liquid to be present in the corner. A small band of high concentration liquid flows through the middle of the container towards the interface, like with container 5 on Texus-32. However, in the end low concentration liquid starts to flow up through the middle of the container (see figure 21f).

Maximum velocities at the interface were 0.5-0.6 cm/s, and 0.25 cm/s normal to the interface between the two roll cells. The centres of the roll cells were located at roughly 0.15 cm from the interface.

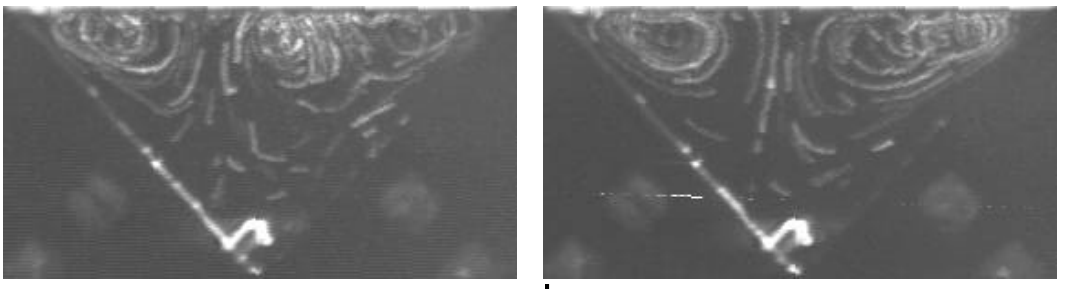

figure 20 *Roll cell pattern in container 1 (reference experiment) between 15-20 seconds (a) and between 25-30 seconds (b). Video frames have been added for 5 seconds.*

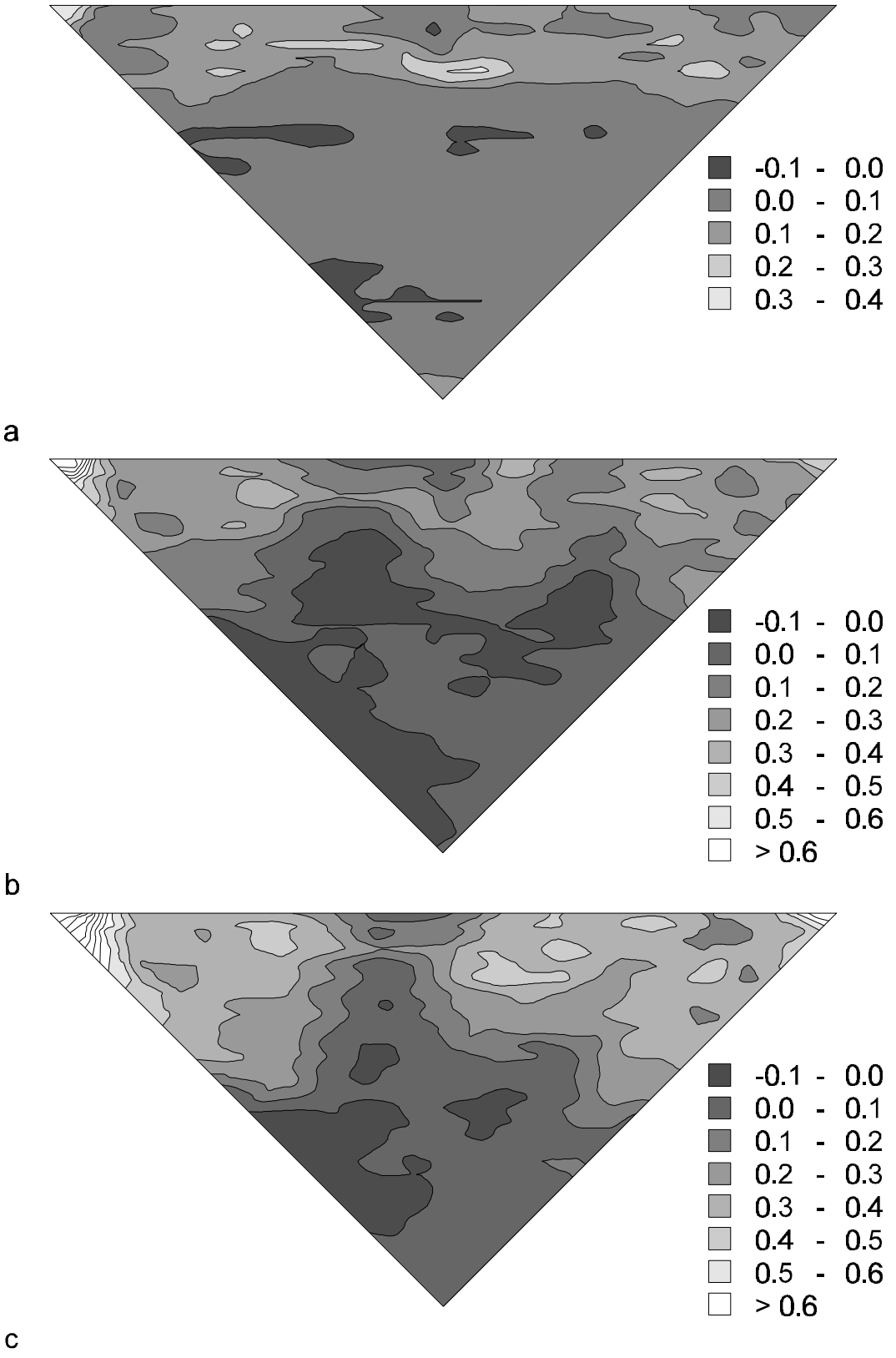

figure 21 *DO.P.D. maps of container 1 (reference experiment) after 4 seconds (a), 13 seconds (b) and 20 seconds (c).*

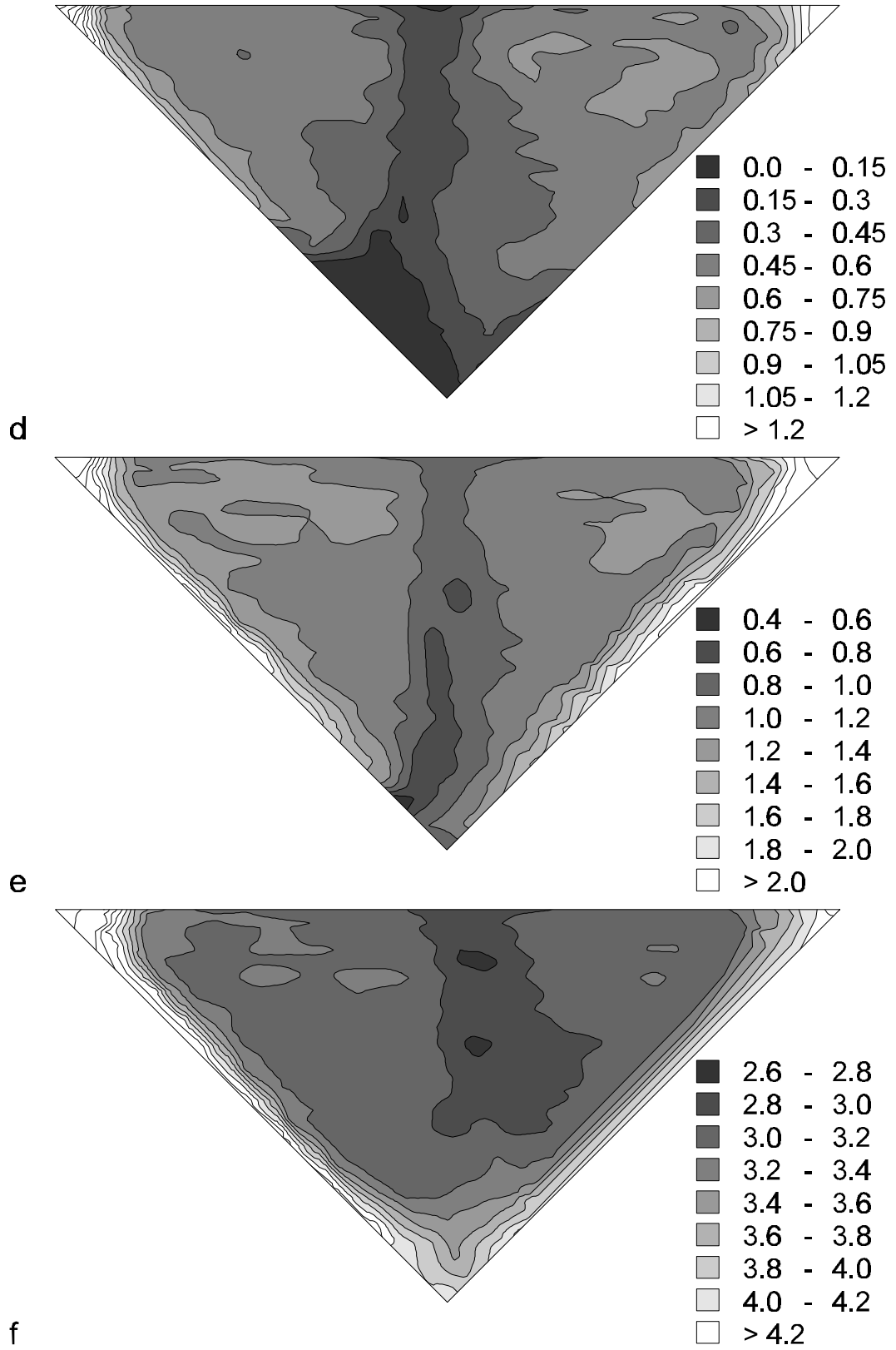

figure 21 DO.P.D. maps of container 1 (reference experiment) after 40 seconds (d), 121 seconds (e) and 294 seconds (f).

After 294 seconds, the liquid was rejected, as was done during microgravity. Then, the liquid was injected and rejected again for a couple of times. More or less the same pattern was obtained in these cases. Not in every case, however, four roll cells were seen distinctly in the period directly after injection. Also in other tests, the four roll cell pattern was observed only occasionally. Whether two or four roll cells can be observed, therefore, can not be predicted for this geometry and this concentration. The formation of four roll cells can be looked at in two different ways. Firstly, it can be regarded as a consequence of the initial microconvection. As seen from the container 4 and 7 experiments, four roll cells is the preferred mode in which microconvection develops. As soon as the macroconvection takes over, two roll cells emerge. From another point of view, it can be argued that an initial macroconvective roll cell, which is confined to the corner, lowers the interface concentration where the liquid from the bulk rises to the surface. This could drive a counter rotating roll cell. However, the latter argument is invalidated by the observation that the four roll cell pattern was never observed when the interface was partly polluted, i.e. when the convective pattern is dominated by macroconvection.

Reference experiment container 5 (4.83 wt %)

Recall that the difference between container 1 and 5 is the width of the container: 0.5 and 1 cm respectively. The experiment with container 5 starts off with a slight bending of the fringes near the interface, but much less obvious than was the case for container 1. Although unordered convection can be seen at the interface penetrating roughly 0.15 cm for the first few seconds, two large roll cells start to develop from the corners almost directly. After 25 seconds, a stream high concentration liquid coming to the interface can already be distinguished in the interferograms. A small roll cell rotating in the same direction as the large roll cell is present in the right corner (see figure 23a). Heavy liquid rolls down the solid side walls to the bottom of the container and this process reverses the concentration distribution in the container. After 240 seconds, the liquid that flows up in the middle of the container, is not any longer relatively rich in acetone, but relatively poor. This is illustrated nicely in figures 22f and 22g. When interpreting these figures, it should be noted that due to the orientation of the fringes the representation of the low concentration liquid at the solid walls is quite poor in the ΔO.P.D. maps. Qualitatively, the interferograms themselves illustrate this point better (figures 22a, b). The inversion of concentration distribution (i.e. acetone-poor liquid present in the bottom rather than in the top of the container) was also observed in some more lengthy experiments with container 1. This inversion of concentration distribution due to Rayleigh convection is the most distinct difference between microgravity and normal gravity experiments.

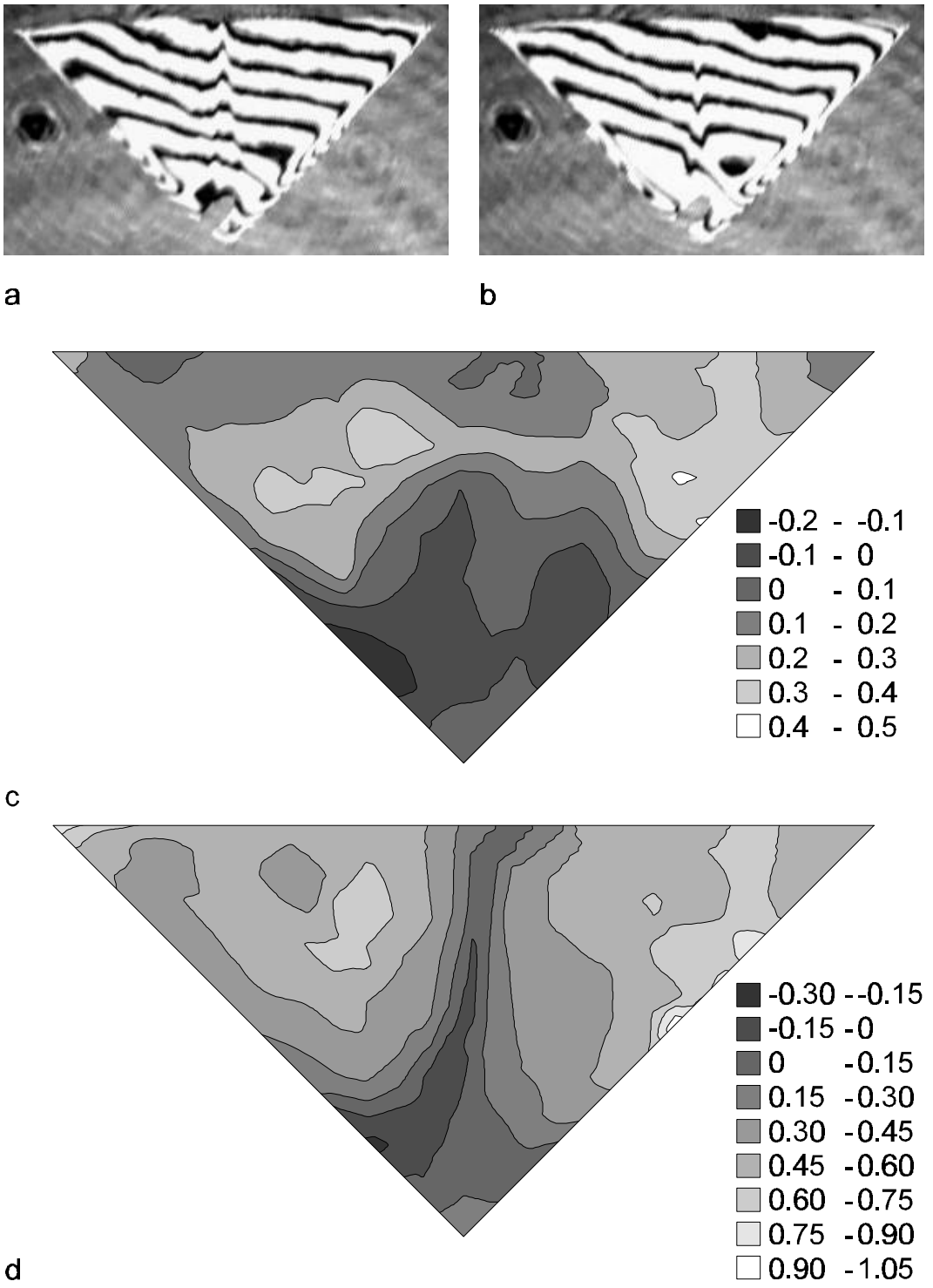

figure 22 Interferograms and DO.P.D. maps of container 5 (reference experiment) after 181 seconds (a), 294 seconds (b), 13 seconds (c) and 30 seconds (d).

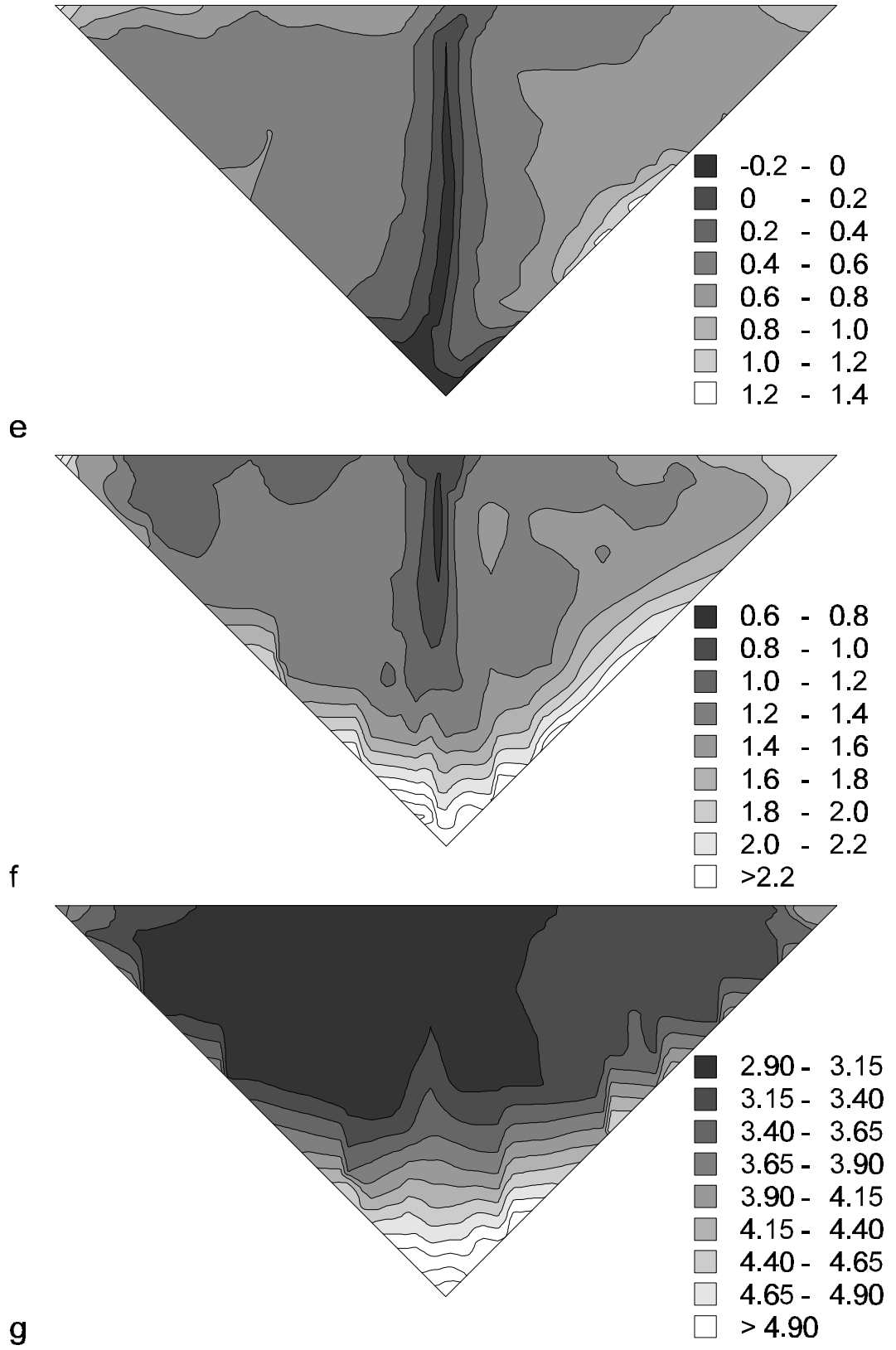

figure 22 DO.P.D. maps of container 5 (reference experiment) after 70 seconds (e), 181 seconds (f) and 294 seconds (g).

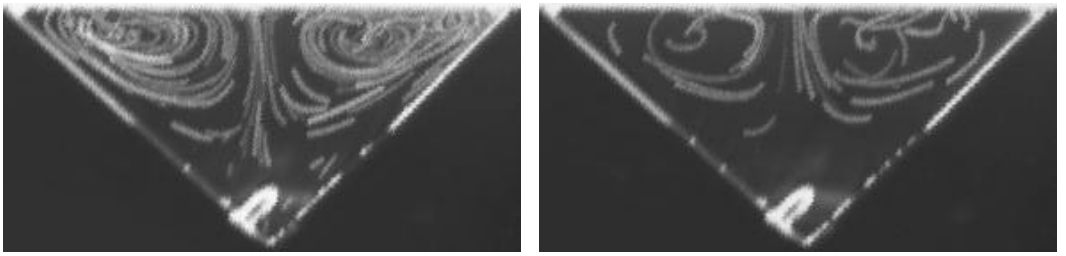

figure 23 Roll cell pattern in container 5 (reference experiment) between 25-30 seconds (a) and between 175-180 seconds (b). Video frames have been added for 5 seconds.

The ΔO.P.D. values in the bulk are slightly larger than the values for container 1, but they are not twice as high, which could be expected from the double width of container 5. This can be partly explained by realising that the average ΔO.P.D. value over the entire container is lower in the case of container 5, since much more low concentration liquid has penetrated to the bottom of the container as a result of Rayleigh convection. However, it is thought that this can not be the only explanation for the large difference between the two containers. Another explanation is that mixing further away from the interface and normal to the viewing plane is relatively poor in a wider container. This hypothesis, however, is hard to prove.

Again, maximum velocities at the interface are roughly 0.5-0.6 cm/s and the velocity normal to the interface in the middle 0.25 cm/s, occasionally 0.3 cm/s. After rejecting and re-injecting the liquid, the same concentration and flow patterns were observed. This was done a few times. During the periods after re-injection, it was observed that the flow pattern of two about equally large roll cells was disturbed by the inversion of concentration distribution. The middle line between the roll cells started to shift, and, when the experiment was extended for a longer time, tracers behaved anomalously when arriving at the interface. They started to move normal to the viewing plane and in small rolls close to the middle line before being swept away to the right or the left. The interface velocities also seemed to decrease a little. The middle line shifted slowly right and then left again. The most probable explanation is that the inversion in concentration distribution due to Rayleigh convection reduces the concentration gradient parallel to the interface. This results in smaller velocities and a larger chance that instabilities in the bulk flow change the position of the middle line between the roll cells.

Reference experiment container 1 (9.97 wt %)

In this experiment, the acetone concentration was doubled. Only a few tracers were present. However, from the interferometry it is clear that the initial flow pattern consists of four roll cells (see figure 25a, b). After 30 seconds, a two roll cell pattern emerges. Qualitatively, the same concentration distribution is observed as in the reference experiment with 4.83 wt %. However, the ΔO.P.D. values are roughly twice as large. This is also anticipated as the concentration is twice as high. Measured maximum velocities also range higher. Especially after rejection and re-injection, but also before, interface velocities as high as 1.2 cm/s are sometimes measured. The flow is much more intense. In the four roll cell stage a tracer is observed to be kicked from the interface into the bulk between the two roll cells in the centre with a speed of 0.65 cm/s. Also with other tests with 10 wt % acetone, maximum interface velocities over 1 cm/s were observed.

The larger driving force for evaporation results in higher concentration gradients parallel to the interface and therefore in higher velocities. Since the ΔO.P.D. values are almost exactly twice as high as for container 1 (corresponding to the doubled concentration), it seems that the extra Marangoni convection (twice as high velocities) has hardly increased the relative rate of mass transfer. This can only be explained if, due to the mixing in the liquid phase, the mass transfer is in neither case limited by the liquid phase mass transfer resistance. Experiments with a lower concentration confirm this observation. Without pollution and when Marangoni convection is present, changes in bulk concentration values are roughly proportional to the absolute concentration.

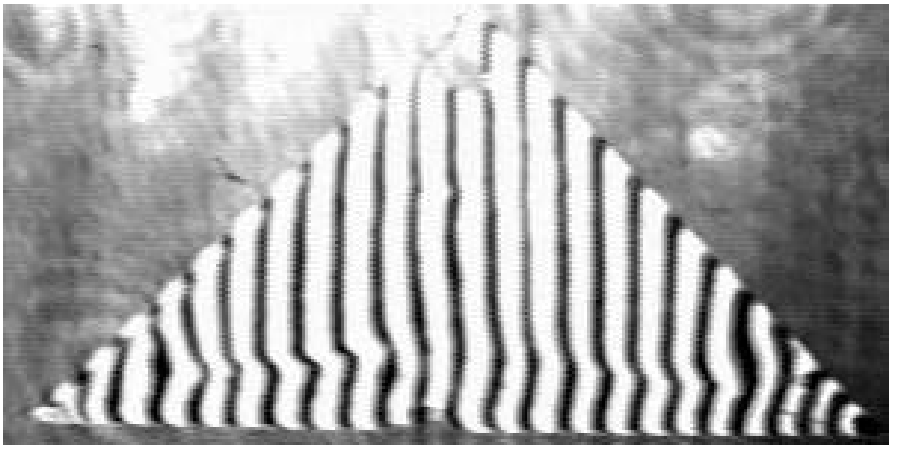

figure 24 Interferogram of container 1 (reference; 9,97 wt %) after 4 seconds.

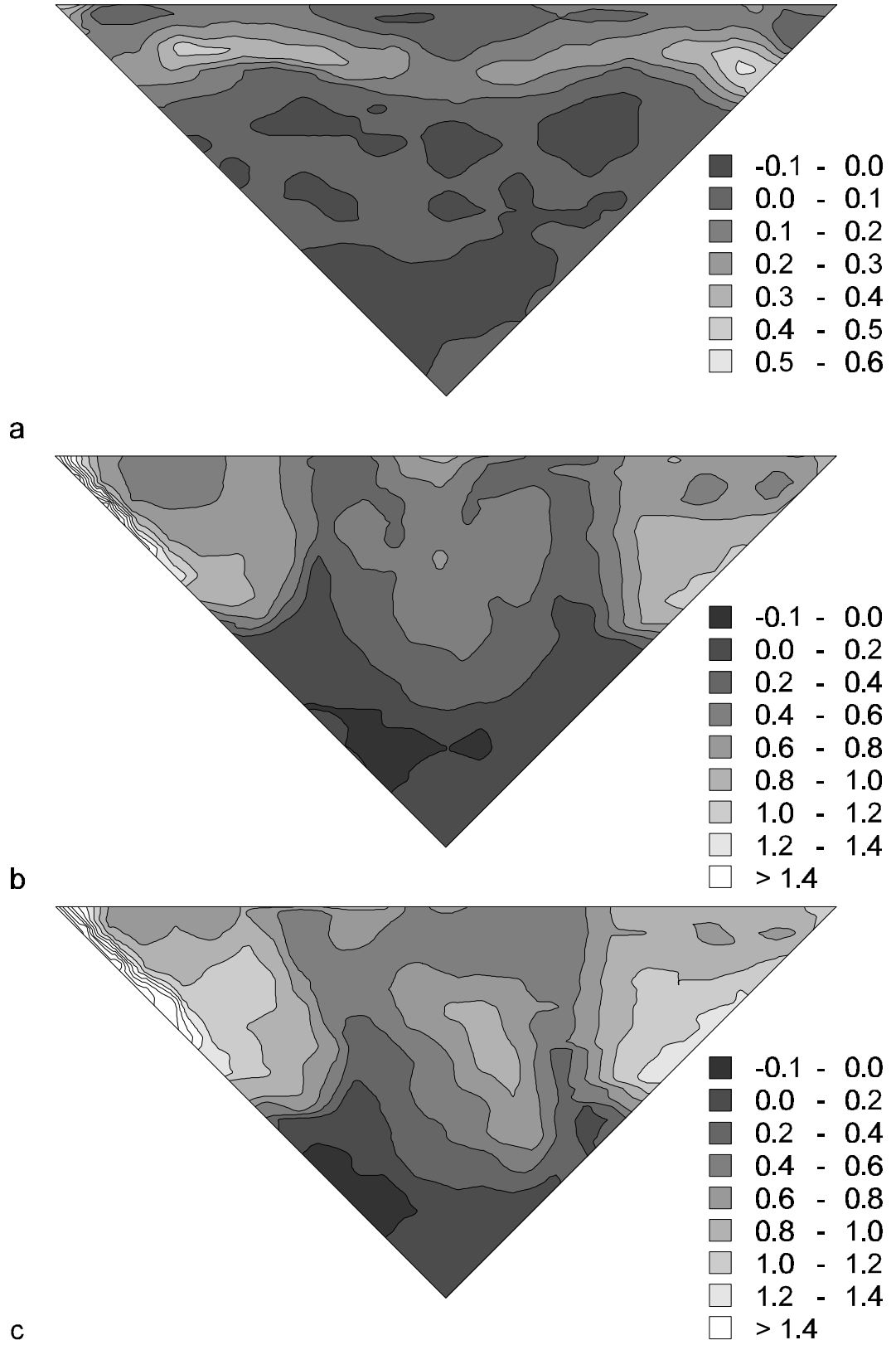

figure 25 DO.P.D. maps of container 1 (reference experiment; 9.97 wt %) after 4 seconds (a), 20 seconds (b) and 30 seconds (c).

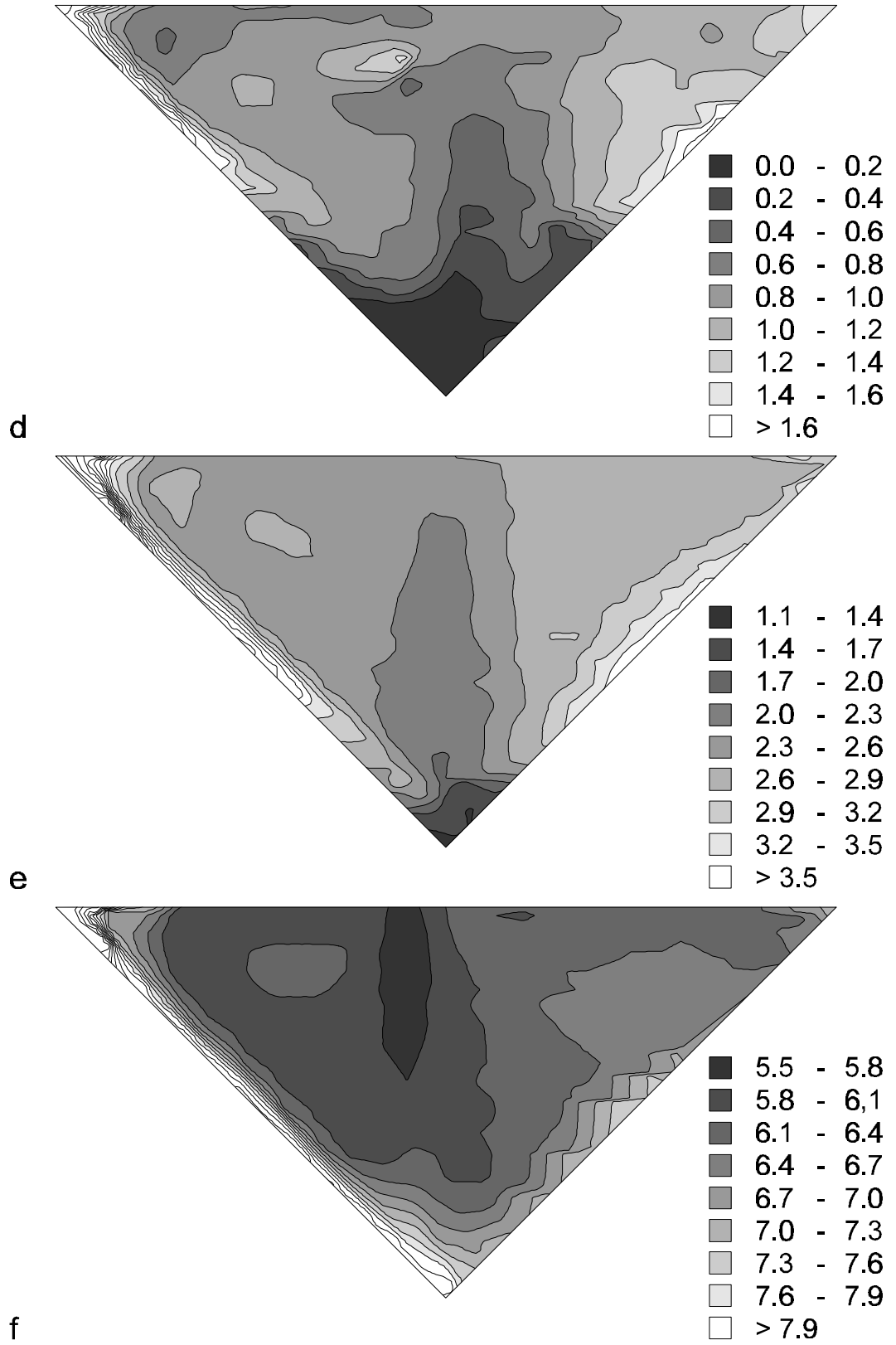

figure 25 DO.P.D. maps of container 1 (reference experiment; 9.97 wt %) after 40 seconds (d), 121 seconds (e) and 294 seconds (f).

Other results

In numerous experiments on earth, pollution manifested itself. On spots at the interface where pollution is present, large gradients in concentration can build up. At clean places these gradients are destroyed by Marangoni convection. When large enough gradients have built up at the polluted spots, 'tears' of heavy liquid roll down into the bulk. The size of these tears is roughly 1-2 mm and the difference in O.P.D. between the bulk and the tears is difficult to measure, but estimated at 1-3. The tears can only be seen in the interferograms and not in the flow patterns. The tears move at a speed dependent on their size and concentration, but typically at a speed of 0.3 mm/s. Similar tear-like gravitational instabilities have been observed by other authors in various systems [7, 23, 24].

In some experiments, no convection was observed initially. Concentration gradients were allowed to build up. Between 15 and 30 seconds after injection a sudden initiation of the flow was observed as tracers were pulled outwards, usually from a spot in the middle. When changing to interferometry after the initiation, tears could be observed at the edges of this 'clean' spot. An example can be seen in figure 26. Obviously, Marangoni convection and Rayleigh convection co-operate to initiate an instability. Linear stability analysis shows that the larger the Rayleigh number, the smaller the critical Marangoni number and vice versa (see e.g. Nield [25]).

figure 26 *Experiment with 3 wt % acetone, without deldrin pieces as drawn in figure 3. Interferograms after 20 seconds (a) (before initiation of the convection) and 30 seconds (b) (after initiation). Tears can be seen in figure b at the edge of the cleared patch. Fringes are strongly bent very close to the interface.*

From the experiments without the deldrin pieces as drawn in figure 3, it can be concluded that velocities are slightly larger without the confined gas space. When pollution is present, sometimes initiation velocities of more than 1 cm/s can be observed.

The reversed mass transfer experiment represents a system that according to the criteria formulated by Sternling and Scriven should be an oscillatory unstable system, as the ratio of gas and liquid diffusivities and the ratio of kinematic viscosities are larger than one, the former being the largest [2]. With respect to buoyancy the system is completely stable. At injection some (macroscopic) convection was obvious from the interferogram, at least for a part due to the injection. During the experiment no tracers were observed moving. Large gradients in

refractive index could be observed in the interferogram in the form of a grey zone, penetrating in the bulk. The grey area consisted of two zones (see figure 27).

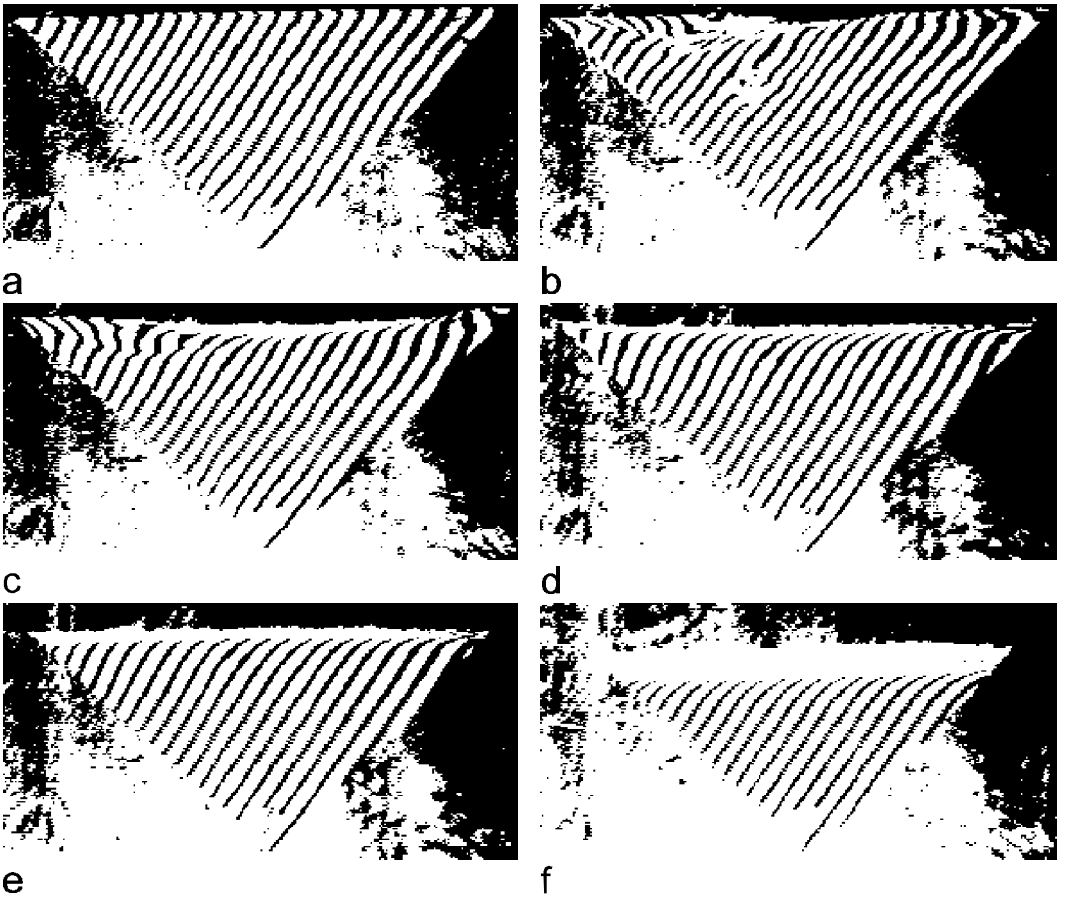

figure 27 The reversed mass transfer experiment before injection (a), directly after injection (b), after 13 seconds (c), after 42 seconds (d), after 118 seconds (e) and after 567 seconds (f).

In the zone close to the interface no interference was observed at all. Deeper in the liquid a zone of a lighter grey existed. In this zone the second light beam (see figure 7) penetrated, but the fringes are too close together to observe. After 118 seconds the light zone had penetrated 1.3 mm and the dark zone 1.0 mm, while after 567 seconds these distances were 3.7 and 2.1 mm respectively. According to the penetration theory the penetration depth should be 0.69 (118 s) and 1.5 mm (567 s). The larger penetration depth in the experiment should be due to very small (macroscopic) flows. The interferograms after short times show that the penetration of the grey zone is larger in the middle than in the corners. This points to flows due to Marangoni convection (as they are exactly the other way around as with the other experiments). Upon rejection and partial re-injection, the interface became visible and tracers were observed to move at a very small speed. Once, oscillatory behaviour with a large wavelength was observed upon re-injection. This could be partly due to large concentration gradients in the liquid upon re-injection. The oscillatory movement damped out in a few

seconds. Although the experiment is interesting in itself, it has no practical significance in mass transfer, as, in negative systems [26] like this, film instability is far more important than any (oscillatory) convection in the film that might or might not increase mass transfer rates. Initial experiments by Linde et al. [22] on the absorption of acetone in water revealed no oscillatory convection either. Later, Linde et al. repeated their experiments, and found oscillatory instability only in case the system was made extremely clean [27]. Ellis and Bidulph found similar oscillations (ripples) on absorption of acetone in water and argued in a similar way on its influence on mass transfer [28]. Therefore, the experiment was not repeated.

2.6 Results from parabolic flight experiments

The parabolic flight experiments mainly served to technically prepare the sounding rocket experiments. Some observations that have not been mentioned before are reported here.

In container 6, convection was observed frequently. Two small roll cells were observed after a very short time. In one case two roll cells emerged that produced an O.P.D. change in the roll cell area of 0.5-1 after only 10 seconds. Also in container 8 convection was sometimes observed, but less intense as for container 6. Container 8 was clearly more sensitive to pollution as container 6.

In container 7, microconvection was observed during microgravity. In two cases, liquid was left to stay in this container in such a way, that the liquid did not overflow the rims during normal or increased gravity. In this way a flat interface with meniscus was created. Interferometry could be observed during both microgravity as well as 1 g or 1.8 g - periods. Due to partial pollution, tears could be observed, but also a typical two roll cell pattern, due to Marangoni convection, emerged. During increased gravity periods, tears were observed to fall down at speeds between 0.06-0.09 cm/s, occasionally even 0.15 cm/s. At normal gravity levels these velocities were between 0.03 and 0.06 cm/s. During microgravity, concentration gradients due to tears were smoothed out by Marangoni convection.

In one case, container 1 was polluted so much that no Marangoni convection was seen, even during normal or increased gravity periods. Tears were observed across the whole interface. However, also two roll cells resulted, driven by Rayleigh convection, as could be concluded from the fact that no tracers were accelerated at the interface. These Rayleigh roll cells turned the same way as Marangoni roll cells and penetrated deeply into the bulk. One tracer was observed to move at an average speed of 0.02 cm/s at the outer edge of one of the roll cells.

2.7 Discussion

From the experiments it is clear that microconvection in the V-shaped geometry always leads to a final macroscopic flow pattern, consisting of two roll cells. The flow and concentration patterns of container 4 (convex surface) and 5 (flat surface) have much in common. The discrimination between micro- and macroconvection is only useful when referring to the initial flow pattern. This flow pattern is dominated by macroscopic

concentration gradients in the case of macroconvection and in the case of microconvection it is dominated by concentration gradients as a result of instabilities. In the reversed mass transfer experiment, macroconvection is the only observed mode of Marangoni convection. For container 1 (flat surface), the initial flow pattern sometimes seems to be a hybrid between micro- and macroconvection. From the experiments it is clear that a four roll cell pattern is the preferred initial mode in the case of microconvection. For a more detailed discussion one is referred to the discussion for container 4 in section 2.4.

The analysis by Bakker et al. [29] for Marangoni instabilities in liquid-liquid systems predicts that the characteristic roll cell size is never much more than the penetration depth of the solute. Applied to the system under investigation, this analysis would predict much smaller roll cells than are found experimentally, since the diffusivity of acetone in water is $1.27\ 10^{-9}$ m^2/s. Even after 300 seconds, the penetration depth of the solute is not more than 1 mm, while the actual roll cell size is 1 cm. It is, however, important to realise that the gas phase diffusion coefficient of acetone is also relevant for concentration gradients parallel to the interface. Since the gas diffusivity is $1.04\ 10^{-5}$ m^2/s [1], gradients at the interface have penetrated 1 cm in only 3 seconds, explaining the relatively large roll cells found. Bakkers analysis applies only if diffusivities in both phases are approximately equal. This seems a trivial remark, but the role of the gas phase diffusion coefficient in gradients parallel to the interface is often neglected, as is the role of the thermal diffusion coefficient in the gas phase (20 times larger than that of the liquid phase) in many Benard problems.

For various experimental reasons, the exact velocities at the interface are difficult to determine. Estimated maximum interface velocities are typically 0.4-0.6 cm/s, but are higher in the case of an increased driving force for evaporation and directly after initiation of Marangoni convection. The width of the container does not play a role in this respect, as maximum velocities in containers 1 and 5 are approximately equal.

The Marangoni flow is driven by a concentration gradient parallel to the interface. An estimate for the magnitude of this concentration gradient based on the observed interface velocities can be made. Consider the analytical solution of Levich [30] for the interface velocity u_i in the case of Marangoni flow in a thin film of thickness h:

$$u_i = \frac{1}{4\mu}\left(\frac{d\gamma}{dc}\right) h \frac{\partial c}{\partial x} \qquad (16)$$

In this equation, μ is the dynamic viscosity ($1\ 10^{-3}$ Pa s), x the co-ordinate parallel to the interface, and $(d\gamma/dc)$ is the dependence of surface tension on concentration ($-1.6\ 10^{-4}$ m^3/s^2). In order to compare Levichs case with ours, the film thickness has to be substituted with the distance from the interface to the centre of the roll cell. When a maximum velocity of 5 mm/s is assumed and h is set to 0.15 cm, the interface concentration change per cm is calculated to be 0.08 wt % (1.2 O.P.D). This is the same order of magnitude as found in the experiments.

The maximum interface concentration in the middle of the container in the case of diffusion can be calculated when both the liquid and the gas phase are assumed to be semi-infinite. The interface concentration $c_{l,i}$ then is [31]:

$$c_{l,i} = c_{l,b}\left(\frac{1}{1+m\sqrt{\frac{D_g}{D_l}}}\right) \qquad (17)$$

In this equation $c_{l,b}$ is the bulk liquid concentration (the bulk gas phase concentration is zero) measured in kg/m^3, m is the distribution coefficient, D_l the diffusion coefficient of acetone in water, and D_g the diffusion coefficient of acetone in air. The distribution coefficient is the ratio between concentration of acetone in liquid and the concentration of acetone in air at equilibrium. When values of $1.60\ 10^{-3}$ for m [32], $1.27\ 10^{-9}$ m^2/s for D_l and $1.04\ 10^{-5}$ m^2/s for D_g are used, this maximum interface concentration is 4.24 wt %. This corresponds to an O.P.D. change of roughly 9 with respect to the bulk. If mass transfer in the gas phase can be described by the film theory (which is the case after a few seconds) this O.P.D. change is even larger. However, in the middle of the containers, in the case of Marangoni convection, fringes always extended almost straight to the interface (as closely as the interface could be observed in the interferograms). Only in the case of pollution, fringes were bent significantly close to the interface. Admittedly, the actual interface concentration is not observable from the interferograms, but a difference of more than 1 or 2 O.P.D. seems very unlikely, as no gradients were seen at the interface during rejection, either.

This observation justifies the conclusion that the mass transfer resistance in the liquid phase has been very substantially reduced by the Marangoni convection. Also the comparison between the 9.97 wt % and 4.83 wt % reference experiments in container 1 (section 2.5) leads to this conclusion.

Unfortunately, only experiments with container 1 and 5 could be repeated on earth. This raises questions with respect to the reproducibility of the other experiments. In the case of container 4 it should be said that after careful analysis of the parabolic flight experiments of Hoefsloot et al. [3], a four roll cell pattern was also observed within 10 seconds after injection. In the case of container 7, the final roll cell pattern on FSM-D also consisted of two roll cells. Since both container 4 and 7 exhibited the same flow characteristics, the results seem reliable and also compare very well to the numerical solutions obtained in chapter 3.

2.8 Conclusions

In microgravity, the evolution of solutal Marangoni convection in the systems described can be generalised for two types of containers. Containers that are shaped in such a way that concentration gradients parallel to the interface are created in these containers (macro-containers) should be distinguished from containers that do not induce such gradients (micro-containers). In macro-containers (1, 3, 5, 6), two roll cells form, in some cases preceded by a short-lived four roll cell pattern. These patterns form as soon as the macroscopically induced convection takes over the initial microconvection. In this initial phase, roll cell patterns

oriented normal to the viewing plane prevail for thin containers. The two roll cell pattern consists of two equally sized roll cells and these roll cells transport liquid with a low acetone concentration from the interface into the bulk along the solid side walls and transport liquid with a high acetone concentration from the bulk to the interface in the middle. This roll cell pattern is very stable.

For micro-containers (2, 4, 7, 8), a roll cell pattern of four roll cells emerges from the initial microconvection. This pattern is stable for a period that depends on the size of the container. Due to an inequality in the size of the roll cells, one of the centre roll cells grows on the expense of the other central roll cell and a two roll cell pattern forms. This roll cell pattern has the same characteristics as the one found in the macro-containers.

In gravity, initially the same type of convection is observed. The flow penetrates the bulk deeper than in microgravity and heavy liquid falls to the bottom of the container. From there, this low-acetone liquid is transported to the interface by the Marangoni roll cells and an inversion of the concentration distribution results (i.e. the lower concentration liquid at the bottom, the higher concentration liquid on top). This roll cell pattern is less stable than the one found in microgravity.

Pollution can result in (partial) absence of convection in microgravity. In gravity, pollution initiates buoyancy that manifests itself in the formation of tears. Marangoni convection is able to minimise concentration gradients at the interface, as observed from the almost straight interference fringes at the interface, and therefore increases mass transfer rates (see chapter 4). In a reversed mass transfer system, no microconvection was observed, but very small flows seem to be present.

From the experiments described it is clear that interferometry is a valuable technique to get insight in (bulk) concentration patterns. It is also a valuable indirect means of establishing the exact flow pattern, as this can not always be done from tracer studies alone.

Literature

[1] H.W. van der Klooster, “The influence of gradients in surface tension on the mass transfer in gas liquid systems”, Ph.D. thesis, University of Groningen, 1978

[2] C.V. Sternling, L.E. Scriven, “Interfacial turbulence: hydrodynamic instability and the Marangoni effect”, A.I.Ch.E. J., 5(4), 514-523, 1959

[3] H.C.J. Hoefsloot, L.P.B.M. Janssen, R.T. Sibbald, H.W. Hoogstraten, “Experimental results from Marangoni convection in V-shaped containers under microgravity conditions”, Microgravity Sci. Techn. IV/1, 55-59, 1991

[4] T. Molenkamp, T.G. Zijlema, L.P.B.M. Janssen, “Determination of flow pattern and concentration distribution as a result of Marangoni convection in V-shaped containers”, ESA WPP-66, 67-70, 1993

[5] F.J. Weinberg, “Optics of flames”, Butterworths (London), chapter 8, 1963

[6] F.I. Kurganova, Yu. A. Redin, V.N. Ermashkevich, M. Kh. Grishchuk, “Study of Marangoni effect with diffraction interferometer”, Theor. Found. of Chem. Eng., 26(6), 746-748, 1992

[7] A.J.M.A. Oyekan, H. Sawistowski, “Interferometric study of gas absorption with chemical reaction”, Chem. Eng. Sci., 26, 1772, 1971
[8] M. Pertler, M. Häberl, W. Rommel, E. Blass, “Mass transfer across liquid-phase boundaries”, Chem. Eng. Proc., 34, 269-277, 1995
[9] L.K. Mudge, W.J. Heideger, “The effect of surface active agents on liquid-liquid mass transfer rates”, A.I.Ch.E. J., 16, 602-608, 1970
[10] S. Miyashita, H. Komatsu, Y. Suzuki, T. Nakada, “Observation of the concentration distribution around a growing lysozyme crystal.”, J. Cryst. Growth, 141, 419-424, 1994
[11] A. Ito, S.K. Choudhury, T. Fukano, “Heated liquid film flow and its breakdown caused by Marangoni convection”, JSME Int. J. ser. II, 33(1), 128-133, 1990
[12] K. Onuma, K. Tsukamoto, S. Nakadate, “Application of real time phase shift interferometer to the measurement of concentration field”, J. Cryst. Growth, 129, 706-718, 1993
[13] E. Hecht, “Optics”, Addison-Wesley, Reading, 1987
[14] L.P.B.M. Janssen, M.M.C.G. Warmoeskerken, “Transport phenomena data companion”, Edward Arnold, London, 1987
[15] L.E. Scriven, C.V. Sternling, “The Marangoni effects”, Nature, 187, 186-188, 1960
[16] J.C. Berg, A. Acrivos, “The effect of surface active agents on convection cells induced by surface tension”, Chem. Eng. Sci., 20, 737-745, 1965
[17] J.H. Lichtenbelt, A.A.H. Drinkenburg, H.A. Dijkstra, “Marangoni convection and mass transfer from the liquid to the gas phase under microgravity conditions”, Naturwissenschaften, 73, 356-359, 1986
[18] H.A. Dijkstra, J.H. Lichtenbelt, “Mass transfer driven Marangoni convection under microgravity”, Appl. microgravity tech. I, 4, 180-187, 1988
[19] H.A. Dijkstra, “Transient Marangoni convection in a square container”, PhysicoChemicalHydrodynamics, 10 (4), 493-515, 1988
[20] H.A. Dijkstra, “On the structure of cellular solutions in Rayleigh-Benard-Marangoni flows in small aspect ratio containers”, J. Fluid. Mech., 243, 73-102, 1992
[21] H.A. Dijkstra, “Mass transfer induced convection near gas-liquid interfaces”, Ph.D. thesis, University of Groningen, 1988
[22] H. Linde, S. Pfaff, C. Zirkel, “Strömungsuntersuchungen zur hydrodynamischen Instabilität flüssig-gasförmiger Phasengrenzen mit Hilfe der Kapillarspaltmethode”, Z. Phys. Chem., 225, 72-100, 1964
[23] R. Brückner, “Instabilities of interfaces and interfacial convection”, Progress in Astronautics and Aeronautics, 52, 111-124, 1977
[24] J.C. Berg, C.R. Morig, “Density effects in interfacial convection”, Chem. Eng. Sci., 24, 937-946, 1969
[25] D.A. Nield, “Surface tension and buoyancy effects in cellular convection”, J. Fluid Mech., 19, 341-352, 1964
[26] F.J. Zuiderweg, A. Harmens, “The influence of surface phenomena on the performance of distillation columns”, Chem. Eng. Sci., 9 (2/3), 89-108, 1958

[27] H. Linde, E. Schwarz, K. Gröger, “Zum Auftreten des Oszillatorischen Regimes der Marangoni-instabilität beim Stoffübergang”, Chem. Eng. Sci., 22, 823-836, 1967

[28] S.R.M. Ellis, M.W. Biddulph, “Interfacial turbulence measurements”, Chem. Eng. Sci., 21, 1107-1109, 1966

[29] C.A.P. Bakker, P.M. van Buytenen, W.J. Beek, “Interfacial phenomena and mass transfer”, Chem. Eng. Sci., 21, 1039-1046, 1966

[30] V.G. Levich, “Physicochemical hydrodynamics”, Prentice Hall, Englewood Cliffs, 388, 1962

[31] R.B. Bird, W.E. Stewart, E.N. Lightfoot, “Transport Phenomena”, Wiley, New York, pp 624-625, 1960

[32] J.H. Lichtenbelt, B.J. Schram, “Vapor-liquid equilibrium of water-acetone air at ambient temperatures and pressures. An analysis of different VLE-fitting methods”, Ind. Eng. Chem. Process Des. Dev., 24 391-397, 1985